Innovative Techniques and Technology

Gary N. Foulks, Editor

En-face Optical Coherence Tomography as a Novel Tool for Exploring the Ocular Surface: A Pilot Comparative Study to Conventional B-Scans and in Vivo Confocal Microscopy

Rachid Tahiri Joutei Hassani, MD, FEBO, LMCC, [1,2] Hong Liang, MD, PhD, [1,2,3] Mohamed El Sanharawi, MD, MPH, [1] Emmanuelle Brasnu, MD, FEBO, PhD, [1,2] Sofiene Kallel, MD, [1,4] Antoine Labbé, MD, PhD, [1,2,3,4] and Christophe Baudouin, MD, PhD, FARVO[1,2,3,4]

ABSTRACT **Purpose: To explore the potential of spectral-domain optical coherence tomography (SD-OCT) using the en-face technology for the imaging of ocular surface diseases and to correlate the findings with in vivo confocal microscopy (IVCM) images. Patients and methods: 113 eyes of 75 subjects with various ocular surface diseases were investigated with the RTVue® anterior-segment en face OCT. En face OCT images were compared to B-scan OCT and IVCM images. Results: Patients with corneal dystrophies, corneal deposits, keratitis, pterygium, conjunctivochalasis, or ocular surface squamous neoplasia and patients who underwent lamellar corneal surgeries were included. En-face OCT images showed ocular surface tissue changes that were not discernible using conventional B-scan OCT. Nevertheless, there was a good correlation with IVCM analysis. Compared with IVCM, the major advantages of en-face OCT included easy operation and rapid image acquisition, with minimal operator experience required. In addition, the non-contact method avoided patient discomfort and external pressure on the globe, which was especially useful in patients with corneal dystrophies, ulcers, or corneal abscesses. Although the resolution of en-face OCT was lower than that of IVCM, it allowed useful overall visualization of corneal lesions due to the larger areas analyzed. Conclusion: En-face SD-OCT is a novel, valuable tool to assess a wide variety of ocular surface diseases. It can provide additional information and new insight into different ocular surface conditions with no corneal contact.**

KEY WORDS **B-scans OCT, corneal adaptor module, en-face optical coherence tomography, C-scans, ocular surface diseases, RTVue®**

Accepted for publication February 2014.

From the [1]Department of Ophthalmology, 3 Quinze-Vingts National Ophthalmology Hospital, Paris, [2]Center for Clinical Investigations INSERM 503, Quinze-Vingts National Eye Center, Paris, [3]INSERM, U968, Paris, F-75012, UPMC Univ Paris 06, UMR_S 968, Institut de la Vision, Paris F-75012; CNRS, UMR_7210, Paris F-75012, France, and [4]Department of Ophthalmology, Ambroise Paré Hospital, AP-HP, UFR Paris-île de France Ouest, University of Versailles Saint-Quentin-en-Yvelines, Versailles, France.

Supported by: Unrestricted grant from the Center of Clinical Investigations 503 INSERM (National Institute of Health and Medical Research), Quinze-Vingts National Ophthalmology Hospital, Paris, France.

The authors have no proprietary or commercial interests in any concept or product discussed in this article.

Single-copy reprint requests to Prof. Christophe Baudouin (address below).

Corresponding author: Prof. Christophe Baudouin, MD, PhD, FARVO, Department of Ophthalmology III, Quinze-Vingts National Ophthalmology Hospital, 28, rue de Charenton, 75012 Paris, France. Tél : + 331 40021308 ; Fax : + 331 40021399. E-mail address: cbaudouin@quinze-vingts.fr

I. INTRODUCTION

Optical coherence tomography (**OCT**) was initially developed in 1991 by Huang et al at the Massachusetts Institute of Technology (Cambridge, MA, USA).[1] It was first used for analyzing the cornea and anterior segment of the human eye in 1994.[2] Since then, anterior-segment OCT (**AS-OCT**) has rapidly become a reliable tool for anterior segment assessment.[3-6] Recently, the development of spectral-domain (**SD**) technology dramatically improved imaging speeds.[6-10] Among all the SD devices, the RTVue® is the first and the only SD-OCT system to be approved by the U.S. Food and Drug Administration for both corneal and retinal imaging.[11]Its high speed

OUTLINE

and resolution allow the acquisition of three-dimensional (**3D**) volumes that make possible the reconstruction of coronal sections, also called *C-scans* or *en-face OCT*.[12,13] The C-scans are oriented in a frontal plane, perpendicular to the optical axis of the eye. They give an instant overview of tissue changes as a two-dimensional transversal slice at any defined depth.

The aim of our study was to investigate the en-face OCT features of a large variety of ocular surface diseases. The observations using this new imaging technique were also compared and correlated with conventional OCT B-scans, in vivo confocal microscopy (**IVCM**), and previously reported histopathological findings.

II. PATIENTS AND METHODS

This observational case series was conducted between November 2012 and June 2013 at the Quinze-Vingts National Ophthalmology Hospital, Paris, France. Written informed consent was obtained and documented from all participants before OCT and IVCM were performed. The study adhered to the tenets of the Declaration of Helsinki and was approved by the Ile-de-France Institutional Review Board for Research on Human Subjects (CCP 5, N° 10793).

A. Subjects

Patients with various ocular surface conditions were recruited for this study. We classified them into five groups: corneal dystrophies and corneal deposits; keratitis; peripheral sterile infiltrate; infectious keratitis; and conjunctiva-associated ocular surface pathology. All subjects underwent detailed ophthalmic examination, including visual acuity measurement, slit-lamp biomicroscopy, and fundus examination. All patients were then photographed and imaged with anterior-segment OCT. IVCM was performed in patients with map-dot-fingerprint dystrophy, Reis-Bücklers dystrophy, cystinosis, amiodarone thesaurismosis, ocular surface squamous neoplasia (**OSSN**), or pterygium.

B. Anterior Segment SD-OCT Imaging

Anterior segment OCT scans were acquired by a single trained operator (R.T.) using the commercially available RTVue® SD-OCT (Optovue Inc, Fremont, CA, USA). According to the manufacturer, this OCT device provides 26,000 A-scans per second, 15-µm transverse resolution, and 5-µm axial resolution in tissue. It uses an 830-nm laser wavelength and has a 2.3-mm imaging depth.[8,14]

Anterior segment scanning was achieved using two adapter lenses. The first one was the short corneal adaptor module (**CAM-S**) or the high-magnification lens, which allows high-transverse-resolution imaging of 10 µm but scans up to only 3×3 mm. The second one was the long corneal adaptor module (**CAM-L**) or the wide-angle lens, which provides wide-field imaging (8×8 mm wide surface) but has lower resolution (15 µm).[14]

The adaptor lens was placed in front of the retinal objective lens to focus the OCT beam on the anterior segment. A set of gooseneck lights was used to illuminate the anterior segment for concurrent video imaging and was also used for fixation of the contralateral eye.

A high-density SD-OCT volume scan was acquired. Then the 3D data were processed to generate C-scans (en-face OCT in the coronal plane) while B-scans (conventional OCT) were derived from transverse sections. 3x3 mm high-resolution B-scans in size were then performed using the CAM-S with image averaging.

C. Anterior Segment SD-OCT Image Analysis

Anterior-segment OCT volumes were visualized using the algorithm version A6, 2, 0, 68. The RTVue® OCT software automatically processed the OCT image. C-scans were automatically determined by two boundaries parallel to the surface. The distance between these two boundaries corresponded to the C-scan thickness. The default value of this thickness was 31 µm, and it was possible to modify it manually. The C-scan was manually swiped to explore the acquired volume from the surface to the depth (Figure 1). Selected en-face images were then evaluated qualitatively for the shape and degree of reflectivity. They were compared

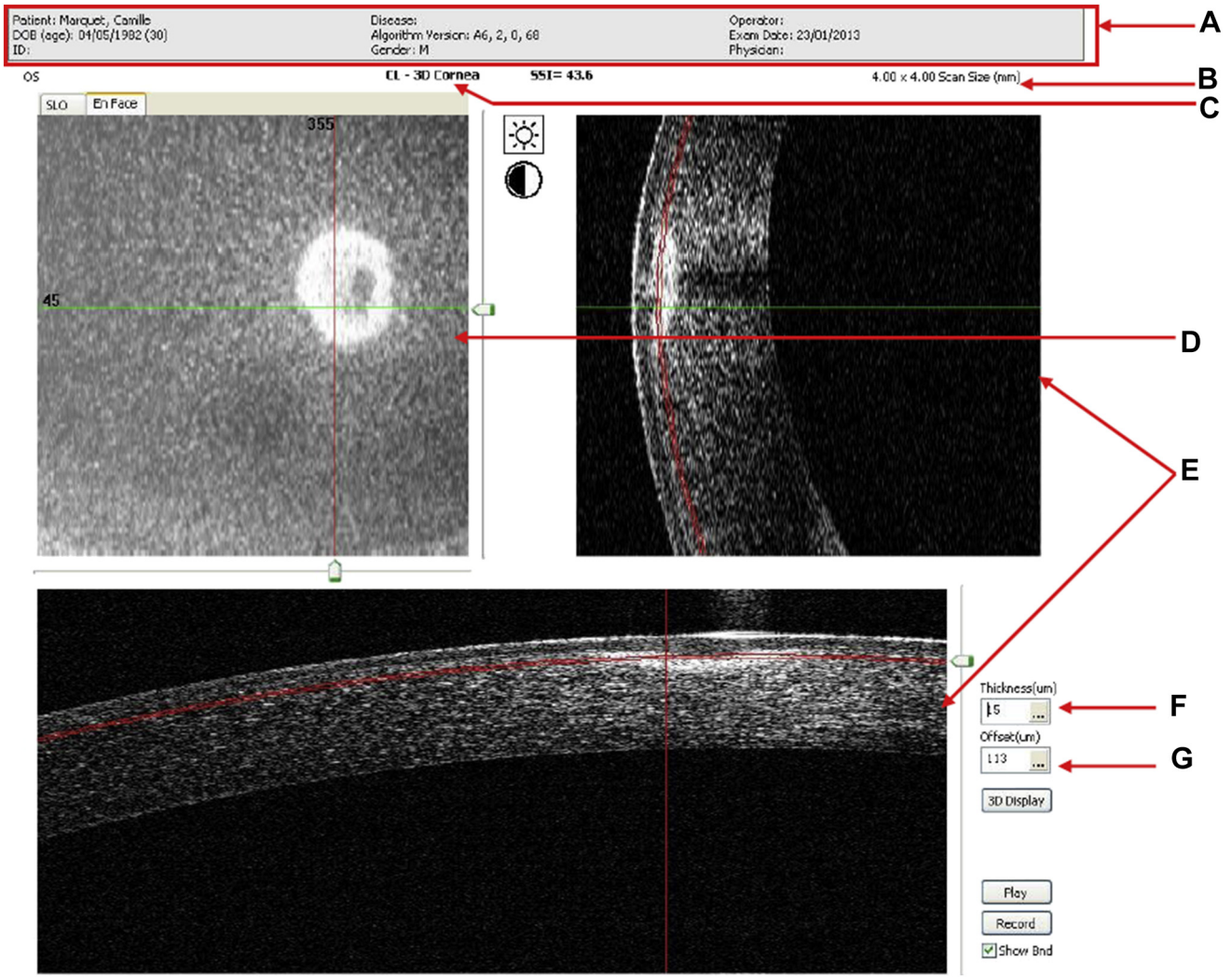

Figure 1. General presentation of en-face OCT printout. The RTVue® en-face OCT printout includes a variety of information, including A) patient's general information, including age, sex, and laterality of eye disease; B) type of lens used (CAM-L or CAM-S); C) surface of the analyzed area (4×4 mm in this example); D): en-face C-scan; E) vertical and horizontal B-scans. The thickness of the C-scan corresponds to the distance between the boundaries. Its default value is 31 µm but it can be manually modified. The depth of the C-scan can be manually adjusted from the surface to the depth.

with conventional data from slit-lamp examination, B-scan OCT, and in vivo confocal microscopy.

D. In Vivo Confocal Microscopy

IVCM was performed using the Heidelberg Retina Tomograph II/Rostock Cornea Module (Heidelberg Engineering GmbH, Heidelberg, Germany) confocal microscope. Before examination, a drop of topical anesthetic (Novesine® 0.4% [oxybuprocaïne 0.4%] MSD-Chibret, Paris, France) and a drop of gel tear substitute (Lacrigel®, carbomer 0.2%, Europhta, Monaco) were instilled. The patient was then seated at an examination table with the head on the headrest. The x-y position of the image and the section depth was controlled manually. The images obtained consisted of two-dimensional high-resolution optical sections covering an area of 400×400 µm, with 2-µm transversal resolution, and 4-µm longitudinal optical resolution. En-face OCT and IVCM images were then compared to identify the same regions in each imaging method.

E. Statistical Analysis

Infectious keratitis areas (in mm^2) were measured in a masked manner by outlining the margins of the abscess using the National Institutes of Health (**NIH**) ImageJ software (Bethesda, MD, USA). The infectious keratitis area was measured at presentation and 7 days after the beginning of antibiotic treatment. Results were expressed as means ± standard error of the mean (**SEM**). Statistical analyses were carried out using GraphPad Prism5 for Windows (GraphPad Software, Inc, San Diego, CA, USA). The paired Student *t*-test was used to statistically evaluate comparisons between pretreatment and post-treatment corneal abscess areas. *P*-values of .05 or less were considered statistically significant.

Table 1. Demographic characteristics of patients included and the features seen in en face OCT scanning.

Diagnosis	Number of subjects	Number of eyes	Age range	Sex ratio	Laterality	Characteristics seen in en-face OCT scanning
Map-dot-fingerprint dystrophy	8	16	25—67	3M / 5W	8R / 8L	Multilaminar, linear, and curvilinear subepithelial hyper-reflective lines.
Reis-Bücklers corneal dystrophy	2	4	9—32	0M / 2W	2R / 2L	Hyper-reflective micro-granular subepithelial deposits.
Salzmann nodular degeneration	1	1	50	0M / 1W	0R / 1L	Nodules appeared as intraepithelial hyper-reflective area.
Cystinosis	7	14	9—67	3M / 4W	7R / 7L	Multiple, hyper-reflective intraepithelial deposits.
Crocodile shagreen dystrophy	1	2	76	0M / 1W	1R/ 1L	Polygonal hyper-reflectivities with indistinct edges, separated by clear lines, predominant in the posterior stroma.
Dry eye keratitis	9	14	35—62	3M / 6W	8R / 6L	Intraepithelial hyper-reflectivity rather than an epithelial defect.
Herpetic keratitis	4	4	22—45	2M / 2W	2R / 2L	Epithelial irregularities and defect. During follow-up, the ulcer resolved by approximation of its edges. An intraepithelial hyper-reflectivity temporarily replaced the ulcer before complete resolution.
Filamentary keratitis	1	1	57	1M / 0W	0R / 1L	Filaments appearing as linear, highly hyper-refllective deposits at the surface of the cornea with posterior shadowing.
Band keratopathy	1	1	59	1M / 0W	1R / 0L	Calcareous deposits corresponding to highly hyper-reflective intraepithelial deposits with posterior shadowing.
Rosacea	4	8	45—69	2M / 2W	4R / 4L	Presence of multiple superficial punctate hyper-reflectivities, which are more frequent in the lower cornea than the upper cornea. Visualization of subepithelial hyper-reflectivities corresponding to subepithelial infiltrate.
Peripheral sterile infiltrate	3	4	25—35	1M / 2W	2R / 2L	Superficial intrastromal hyper-reflectivity of peripheral cornea, with very good visualization of limbal Vogt striae.
Corneal abscess	6	6	21—50	3M / 3W	3R / 3L	A zone of intrastromal hyper-reflectivity. En-face OCT allows visualizing, locating, and measuring the surface of corneal abscess and follow-up of its surface under treatment.
Amiodarone thesaurismosis	1	2	79	0M / 1W	1R / 1L	Visualization of intrastromal linear microdeposits in the anterior stroma.
Pterygium	9	10	27—64	5M / 4W	6R / 4L	Identification of the pterygial borders, stroma, and Fuchs patches in active pterygia.
Conjunctivochalasis	13	21	60—80	6M / 7W	10R / 11L	Visualization of conjunctival cysts with septae.
Ocular surface squamous neoplasia	1	1	64	1M /0W	1R / 0L	Hyper-reflective lesion with clearly visible edges and centred by highly hyper-reflective deposits corresponding to keratinisation.
Corneal grafts	4	4	17—70	2M / 2W	2R / 2L	Assessment of the graft-host interface and lateral junction.
Total	75	113	9—80	33M / 42W	58R / 55L	

L: left; M: men; R: right; W: women.

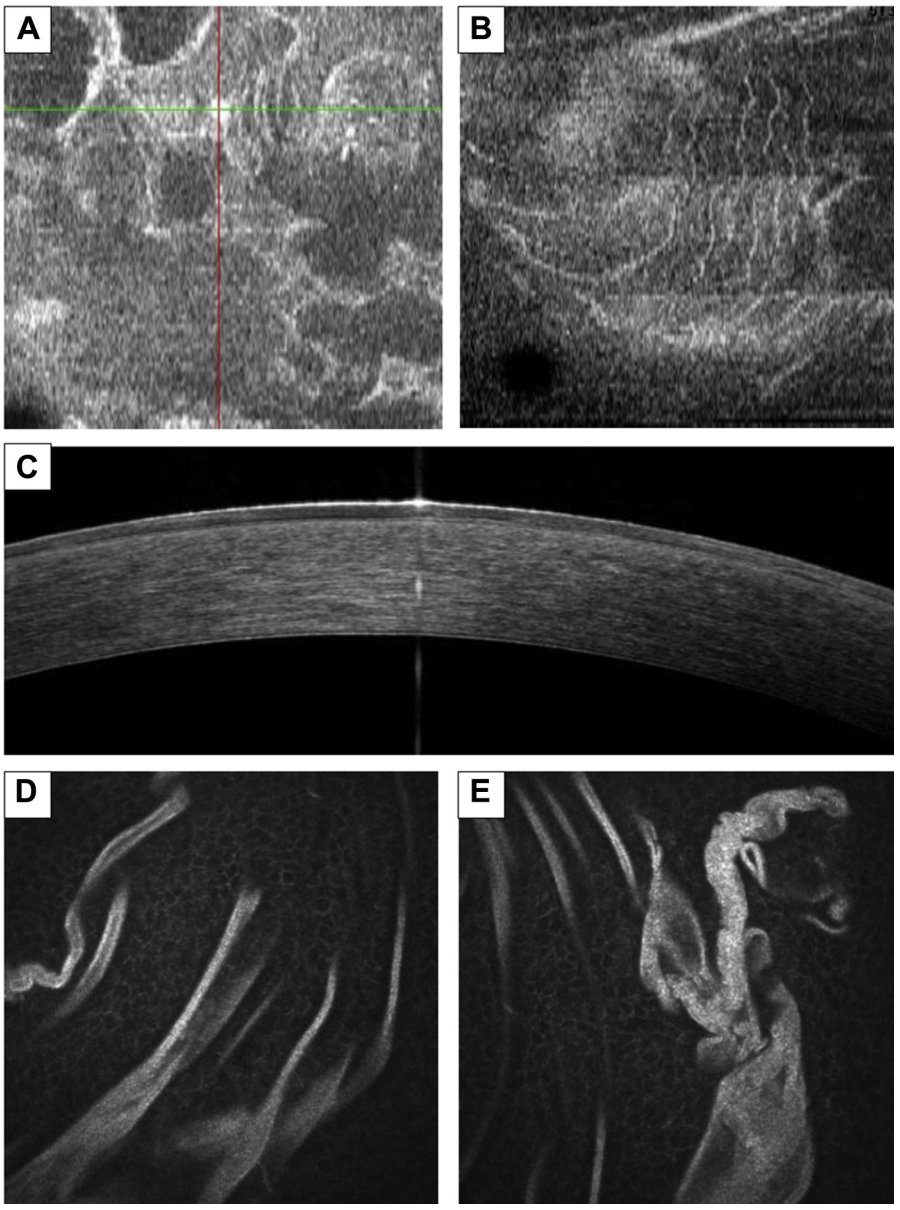

Figure 2. Map-dot-fingerprint dystrophy. (A and B) On C-scans, multilaminar, linear, and curvilinear hyper-reflective lines can be seen. (C) Transversal scan shows discrete irregularities of basement membrane. (D and E) show the corresponding IVCM features.

III. RESULTS

In total, 113 eyes of 75 subjects with various anterior segment conditions were analyzed by anterior-segment SD-OCT combined with IVCM analysis. Fifty-eight were right eyes and 55 were left eyes. The male-to-female ratio was 33:42. Age ranged from 9 to 80 years, with a mean age of 47.4 ± 19.43 years. Table 1 summarizes the characteristics of the subjects included and the characteristic features investigated by en-face OCT scanning. We detailed the different pathologies as shown below.

A. Corneal Dystrophy and Corneal Deposits

1. Map-Dot-Fingerprint Dystrophy

Map-dot-fingerprint (epithelial basement membrane) dystrophy, a bilateral anterior corneal dystrophy, is typically characterized by epithelial fingerprint lines, geographic map-like lines, and dots on slit-lamp examination.[15,16]

Sixteen eyes of eight patients with map-dot-fingerprint dystrophy were analyzed. C-scans showed the presence of typical fingerprint-like, multilaminar, linear, and curvilinear hyper-reflective lines and dots (Figures 2A and 2B). These patterns were especially located in the epithelial basement layer. C-scans were much more obvious than conventional B-scans that showed discrete irregularities at the level of the basement membrane (Figure 2C). En-face OCT scans demonstrated features similar to those observed with IVCM (Figures 2D and 2E).

2. Reis-Bücklers Dystrophy

Reis-Bücklers corneal dystrophy, a dominantly inherited corneal dystrophy, is histopathologically characterized by the presence of band-shaped granular and subepithelial deposits in the Bowman layer.[17] We present the case of a mother (Figures 3A-3C) and daughter (Figures 3D and

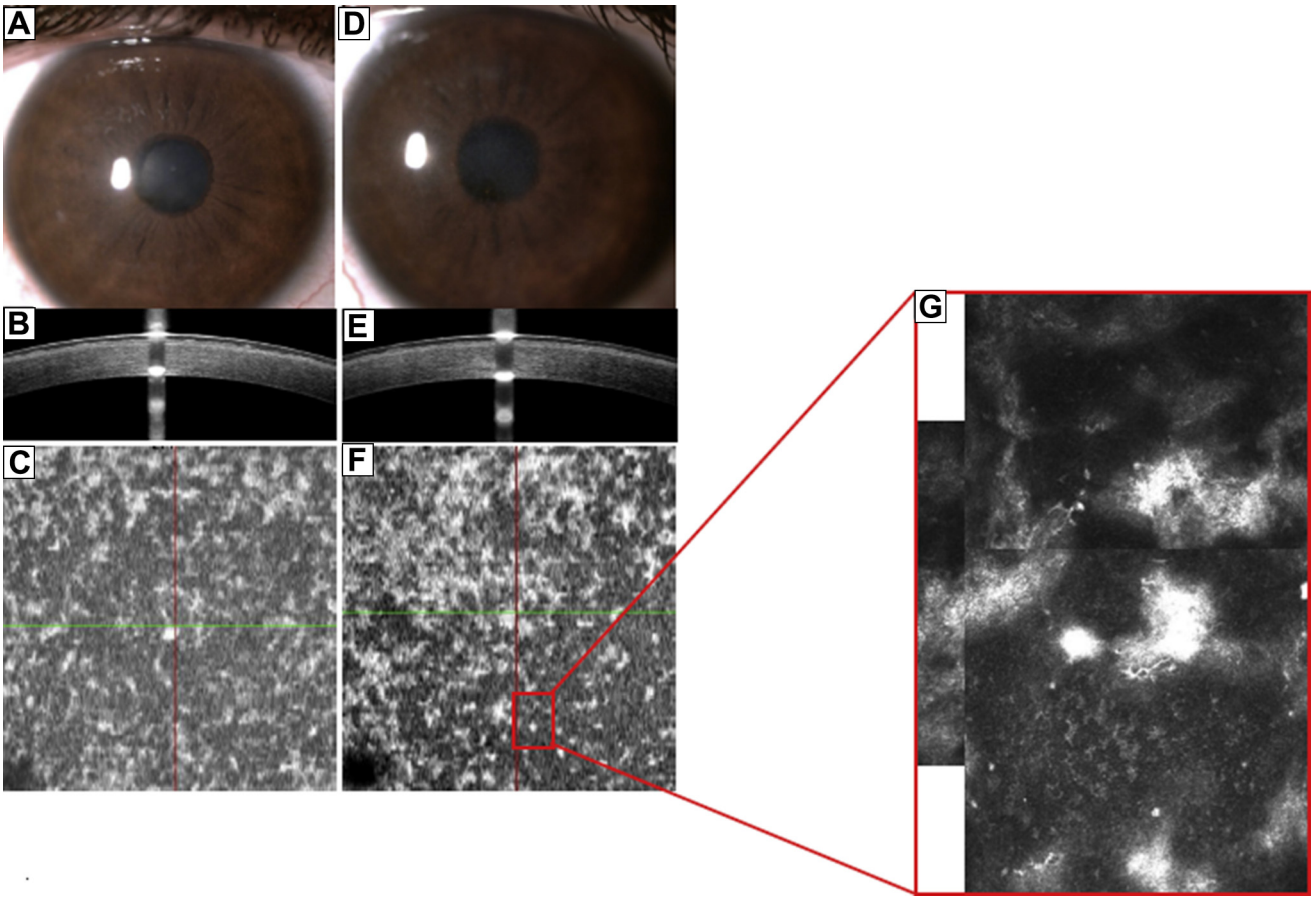

Figure 3. Reis-Bücklers dystrophy. Two cases of Reis-Bücklers dystrophy from one pedigree: a 29-year-old woman (A to C) and her 9-year-old daughter (D to F). Slit-lamp photography (A and D) shows superficial microgranular opacities. B-scan OCT (B and E) shows subepithelial irregularities with the granular subepithelial deposits. En-face OCT clearly shows granular subepithelial deposits (C and F). These features were consistent with those shown by IVCM (G).

3F) with Reis-Bücklers dystrophy. The slit-lamp photograph showed the presence of the subepithelial microgranular opacifications (Figures 3A and 3D). B-scan OCT showed the presence of subepithelial irregularities (Figures 3B and 3E), and the en-face OCT clearly showed the presence of granular subepithelial deposits (Figures 3C and 3F). These features were consistent with the IVCM images in which we observed the presence of nonhomogeneous hyper-reflective materials (50−100 μm) with rounded and hyporeflective edges (Figure 3G).

3. Salzmann Nodular Degeneration

Salzmann nodular degeneration (**SND**) is a noninflammatory, slowly progressive, generally chronic and bilateral corneal dystrophy characterized by single or multiple whitish-gray nodules raised above the corneal surface.[18]

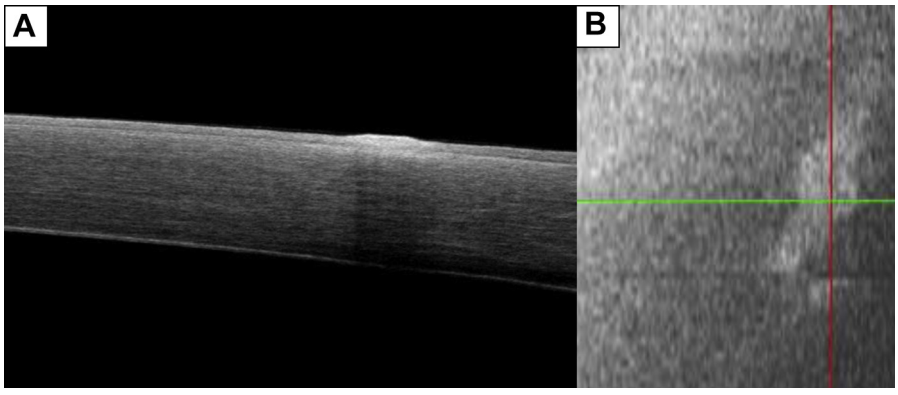

Figure 4. Salzmann nodular degeneration. B-scans (A) demonstrated nodules as hyper-reflective material covered by an abnormally thin layer of epithelium. On C-scans (B), these nodules appeared as an intraepithelial hyper-reflective area.

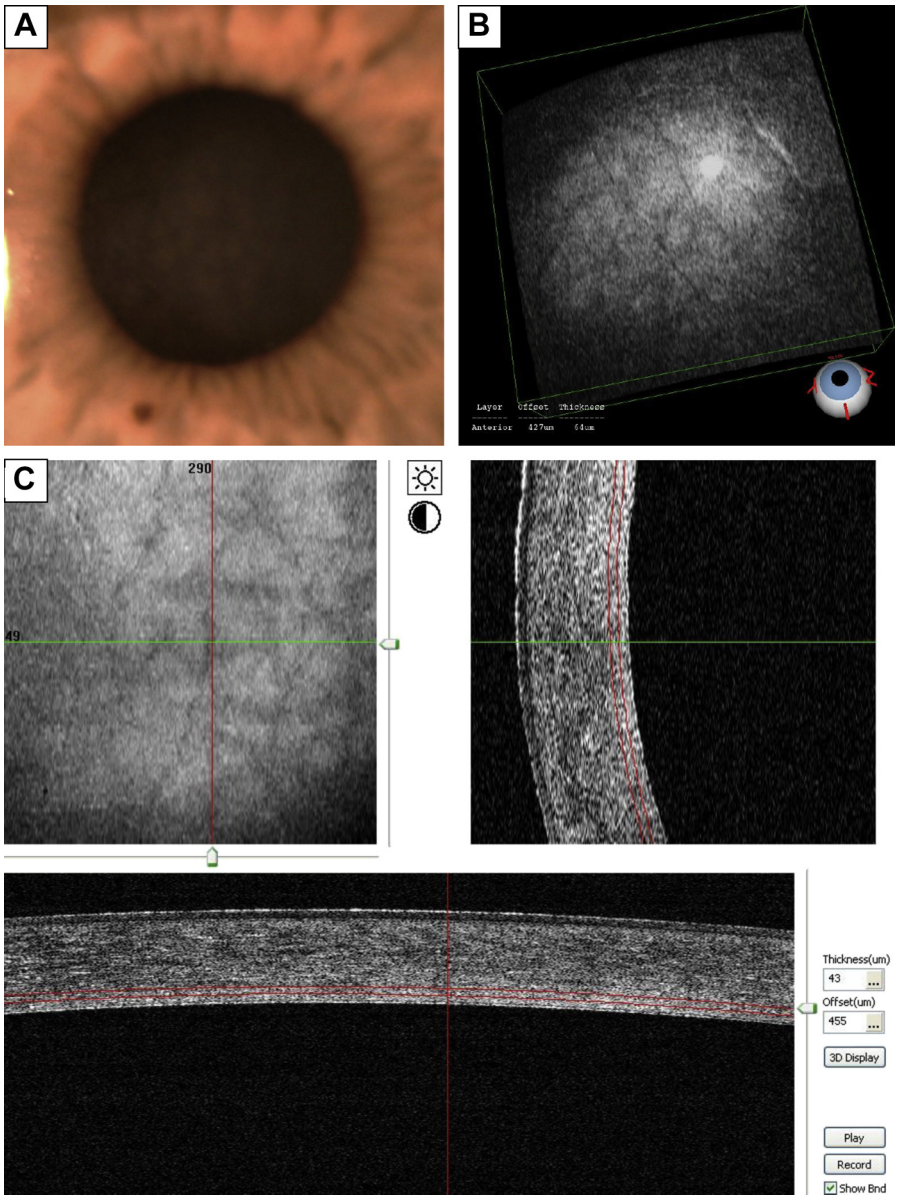

Figure 5. Crocodile Shagreen dystrophy. Slit-lamp examination showed bilateral central opacities in a polygonal pattern with intervening crack-like clear zones (A). These features were visible on deep stromal C-scans (B and C). There were no patent abnormalities on conventional OCT B-scans (D and E).

A 50-year-old woman presented with recurrent pain and irritation in her left eye. Slit-lamp examination showed elevated, whitish-grey subepithelial corneal nodules in the left eye. There was a clear zone separating the outer margin of the degeneration from the limbus. B-scans demonstrated nodules as whitish hyper-reflective material covered by an abnormally thin layer of epithelium (Figure 4A). The infiltrate was accompanied by moderate stromal shadowing. On C-scans, these nodules appeared as intraepithelial hyper-reflective areas (Figure 4B). The surface of the hyper-reflective nodules was about 300×600 µm with an irregular shape. The edges of the nodules were clearly visible.

4. Crocodile Shagreen Dystrophy

Posterior crocodile shagreen dystrophy is characterized by 0.5 to 2.0 µm-diameter lacunae presenting in the corneal stroma and Bowman layer. A saw-toothed lamellar pattern is often evident in the corneal stroma.[19]

A 76-year-old woman presented with bilateral deep central stromal opacities in a polygonal pattern with intervening crack-like clear zones (Figure 5A). There were no patent abnormalities on conventional OCT B-scans (Figures 5D and 5E), but on consecutive OCT C-scans, we were able to visualize polygonal hyper-reflectivities with indistinct edges separated by clear lines (Figure 5B in 3D mode and 5C in en-face mode), which could be the lacunae patterns previously described.[19] This pattern was present only in the posterior stroma, which is consistent with previously reported histological findings.[20]

5. Cystinosis

Fourteen eyes of seven patients were analyzed for ocular cystinosis. The slit-lamp examinations showed the typical

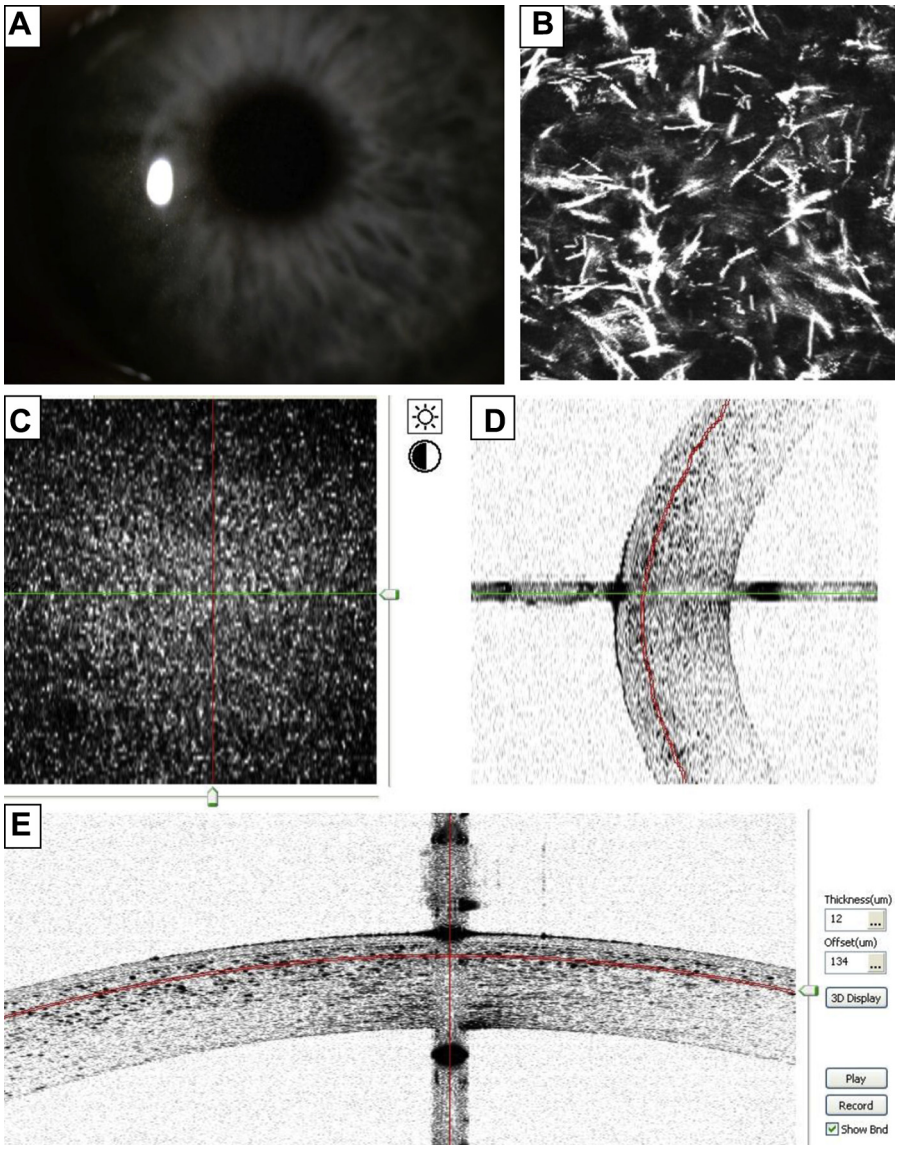

Figure 6. Cystinosis. Slit-lamp examination showed bilateral punctate corneal deposits (A). In vivo confocal microscopy identified intrastromal crystals as spindle, needle-shaped, and fusiform hyper-reflective bodies (B). En-face OCT showed the frontal distribution of these deposits (C), whereas B-scans analyzed their anteroposterior distribution (D and E).

bilateral corneal cystine crystal deposits in all patients(Figure 6A). IVCM identified intrastromal crystals as spindle, needle-shaped, and fusiform hyper-reflective bodies (Figure 6B). En-face OCT showed multiple hyper-reflective deposits in the anterior stroma and made it possible to analyze their distribution throughout all corneal stroma layers (Figure 6C). B-scans revealed hyper-reflective intrastromal deposits (Figure 6D). They were slightly more prevalent in the center than in the periphery of the cornea (Figure 6E).

6. Amiodarone Thesaurismosis

The medical history of a 79-year-old woman revealed that she had undergone chronic amiodarone treatment for 20 years. Slit-lamp examination showed the presence of typical corneal verticillata in both eyes. While conventional OCT scans were not able to visualize these corneal deposits (Figure 7A), en-face OCT (Figure 7B) allowed their visualization and determination of their exact depth (18−40 μm). These corneal microdeposits were present in the anterior stroma and were not found in the posterior stroma. The images were correlated with IVCM images (Figure 7C), which disclosed the hyper-reflective dots with a nonhomogeneous distribution.

B. Keratitis

1. Keratoconjunctivitis Sicca

We investigated 14 eyes of nine patients previously diagnosed with keratoconjunctivitis sicca (**KCS**). Figure 8 shows the profile (Figure 8A) and the en-face (Figure 8B) visualization of dry eye superficial punctate keratitis. Fluorescein-stained areas observed on slit-lamp examination corresponded to intraepithelial hyper-reflective areas on anterior-segment OCT. We observed that positive fluorescein staining spots in dry eye keratitis did not necessarily match epithelial disruption; these spots probably correspond

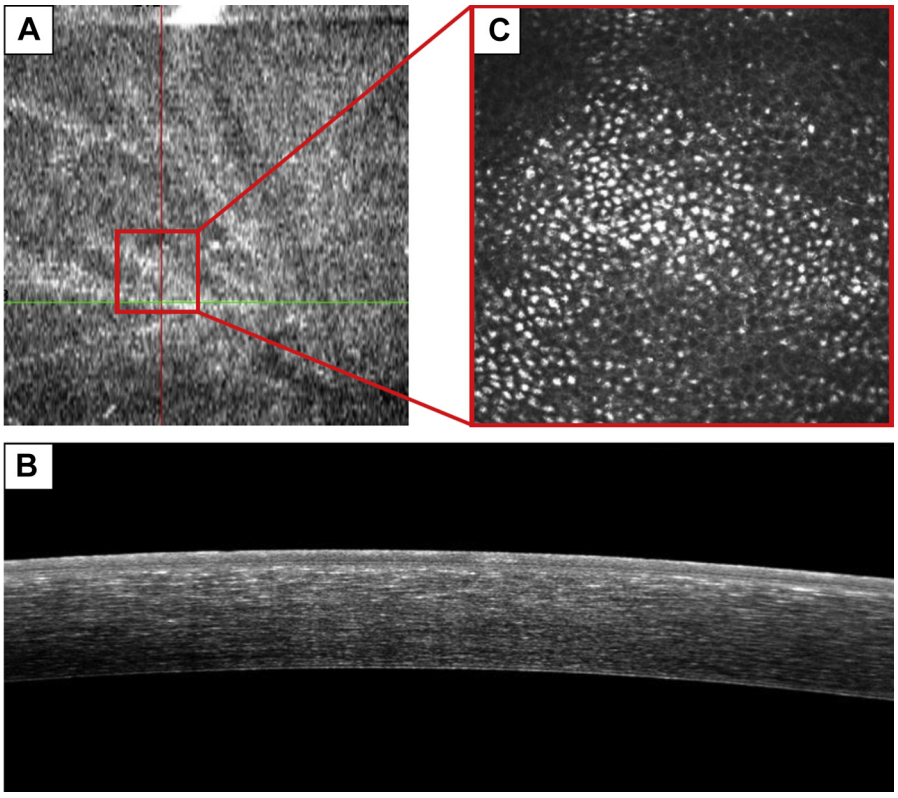

Figure 7. Amiodarone thesaurismosis. Conventional OCT B-scans were not able to visualize these corneal deposits (A) in a patient treated by amiodarone for 20 years. In contrast, en-face OCT (B) was able to analyze and localize the deposits, which were correlated with the in vivo confocal microscopy images (C).

to epithelial cellular damage rather than epithelial disruption.

2. Filamentary Keratitis

A 57-year-old man was suffering from recurrent symptoms of foreign body sensation, discomfort, photophobia, and redness of his left eye. The diagnosis of filamentary keratitis was made based on the clinical findings of positive staining mucus filaments attached at one or both ends to the cornea (Figure 9A). On anterior-segment OCT, the filaments appeared as highly hyper-reflective deposits at the surface of the cornea with posterior shadowing (Figure 9B for the paralleling aspect for one filament and Figure 9C for perpendicular aspects of two filaments). En-face images showed the disposition of filaments (Figure 9D). The epithelial anchorage areas could not be analyzed because of posterior shadowing (Figure 9E).

3. Herpetic Keratitis

Four eyes of four patients with herpes epithelial keratitis were explored. Slit-lamp examination using fluorescein stain revealed a typical dendritic ulcer on the cornea that was indicative of herpes simplex virus infection for all the patients. All patients were treated with acyclovir 3% ophthalmic ointment, applied five times a day for 10 days.

OCT B-scans and C-scans (Figure 10) were taken initially and during the follow-up from day 1 to day 7. Initial fluorescein stained areas observed on slit-lamp examination corresponded to epithelial irregularities and defect. During the follow-up, the ulcer resolved by approximation of its edges. An intraepithelial hyper-reflectivity temporarily replaced the ulcer before complete resolution. En-face OCT allowed the follow-up of the healing process in corneal herpetic ulcer without any direct contact or application of any solutions.

4. Rosacea

Eight eyes of four patients with ocular rosacea and meibomian dysfunction were included in the study. While the orthogonal scans did not show any particular aspect of tear film (Figure 11A), the superficial en-face scans allowed us to visualize superficial lacrimal circular hyper-reflective structures in the precorneal layer (Figure 11B), which were larger and more frequent in the lower cornea than the upper cornea (Figure 11C). En-face OCT in five normal control subjects did not demonstrate these superficial hyper-reflective structures (Figure 11D). Deeper en-face scans allowed us to visualize subepithelial hyper-reflective lesions corresponding to subepithelial infiltrates (Figure 11E).

5. Band Keratopathy

We analyzed a case of band keratopathy in the right eye of a 59-year-old man. On the transversal OCT scan (Figure 12A), we noted the presence of highly hyper-reflective intraepithelial deposits and hyporeflective cysts. En-face OCT showed the distribution of calcareous concretions (Figures 12B to 12E). There was also an intraepithelial hyporeflective area, corresponding to an intraepithelial cyst.

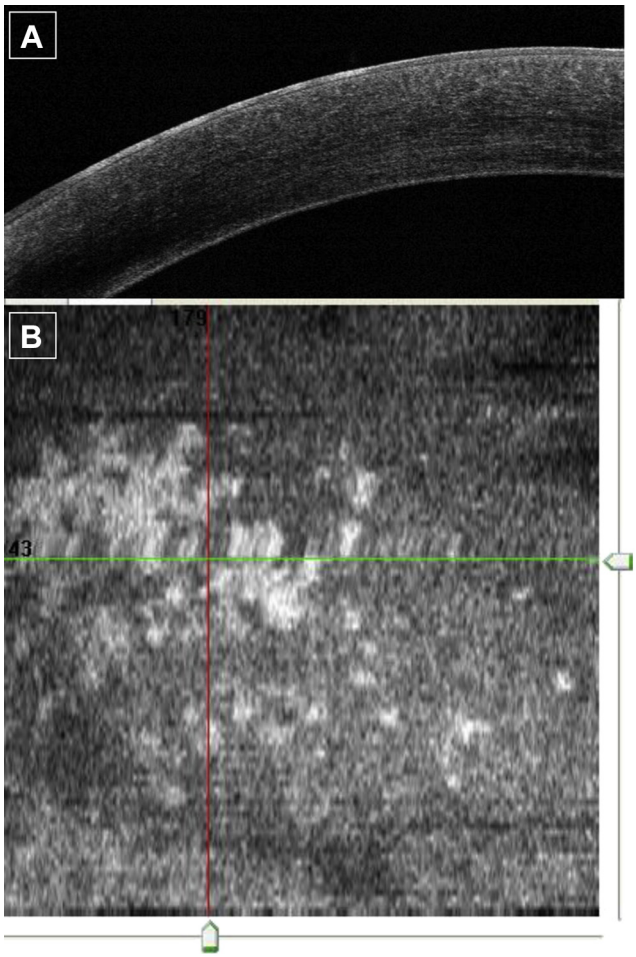

Figure 8. Keratoconjunctivitis sicca. Epithelial hyper-reflectivity areas on B-scans can be seen (A). The coronal distribution of these hyper-reflectivities is clearly visible on C-scans and corresponds to fluorescein stained areas (B).

6. Peripheral Sterile Infiltrates

Four eyes of three patients with peripheral sterile infiltrate were analyzed. In the case shown in Figure 12, a 30-year-old man, a contact lens wearer, presented with discomfort and redness in the right eye. Transversal OCT scans showed the presence of peripheral corneal infiltrate in the anterior stroma (Figure 13A). On en-face OCT (Figure 13B), we noted a superficial circular hyper-reflective area, which corresponded to the peripheral corneal infiltrated area. We clearly visualized limbal Vogt striae close to the infiltrated area, which probably corresponds to immune limbal activation. In other limbus areas far from the infiltrated area, the limbal Vogt striae were not so visible.

7. Infectious Keratitis

Six eyes of six patients suffering from infectious keratitis were investigated with OCT scans. En-face OCT allowed visualizing, locating, and measuring of the surface of infectious keratitis (Figure 14A). In the OCT B-scans (Figures 14B and 14C), the infectious keratitis appeared as an area of intrastromal hyper-reflectivity. At day 1, the average size of the infectious keratitis was approximately 4.99 mm^2 (n=6), and it was reduced to 3.92 mm^2 at day 7 ($P \leq .01$ when compared to day 1). En-face OCT allowed us to monitor the surface of infectious keratitis under treatment without any direct contact to altered areas.

C. Conjunctiva-Associated Ocular Surface Pathology

1. Pterygium

Ten eyes of nine patients suffering from pterygium were analyzed. From the en-face C-scan, the junction of pterygium was clearly distinguished from the normal corneal tissues. In five eyes with active pterygium, we observed hyper-reflective spots in front of the tip of the pterygium (Figure 15A). In contrast, in five eyes with inactive pterygium, there was no hyper-reflectivity in front of the tip of the pterygium (Figure 15B). These findings seen in C-scans correlated with those of IVCM (Figures 15C and 15D). Fuchs patches were associated with pterygium activity.

2. Conjunctivochalasis

We used en-face anterior-segment OCT to analyze 21 eyes of 13 patients with a clinical diagnosis of conjunctivochalasis. In 20 eyes, vertical B-scan showed the presence of a triangular conjunctival fold between lower lid margin and the cornea (Figure 16A, red arrow). On transversal B-scan, there were conjunctival cysts (Figure 16B, red arrowheads). Consecutive OCT C-scans showed superficial linear folds (Figure 16C, yellow arrowheads) and deeper, multiple, hyporeflective conjunctival cysts with septae (Figure 16D, yellow arrows).

In one case of atypical conjunctivochalasis, the vertical B-scan of the conjunctival fold did not show a typical triangular shape, and the vertical section of the conjunctivochalasis was more semicircular than triangular (Figure 17A, red arrow). On transversal B-scans, the cysts were smaller and more circular. Finally, on OCT C-scans (Figures 17C and 17D), the cysts that seemed to be suspended on conventional scans were in fact seen to be organized in a network.

3. Ocular Surface Squamous Neoplasia

A 64-year-old man presented with foreign body sensation, irritation, discomfort and redness of his right eye. Slit-lamp examination showed a translucid, irregular, limbic lesion (Figure 18C). B-scans disclosed thickened hyper-reflective epithelial layer and abrupt transition from a normal to a hyper-reflective epithelium. There were also hyper-reflective superficial deposits with posterior shadowing on transversal scans corresponding to keratinization (Figure 18A). On C-scans, this lesion appeared as a hyper-reflective tissue with clearly visible borders (Figure 18B). These findings were correlated with IVCM images (Figure 18D), which showed hyper-reflective, irregular, multinuclear cells with a clear transition between the normal and abnormal corneal normal epithelium. The diagnosis of ocular surface squamous neoplasia was later confirmed by histopathologic examination of the excised lesion.

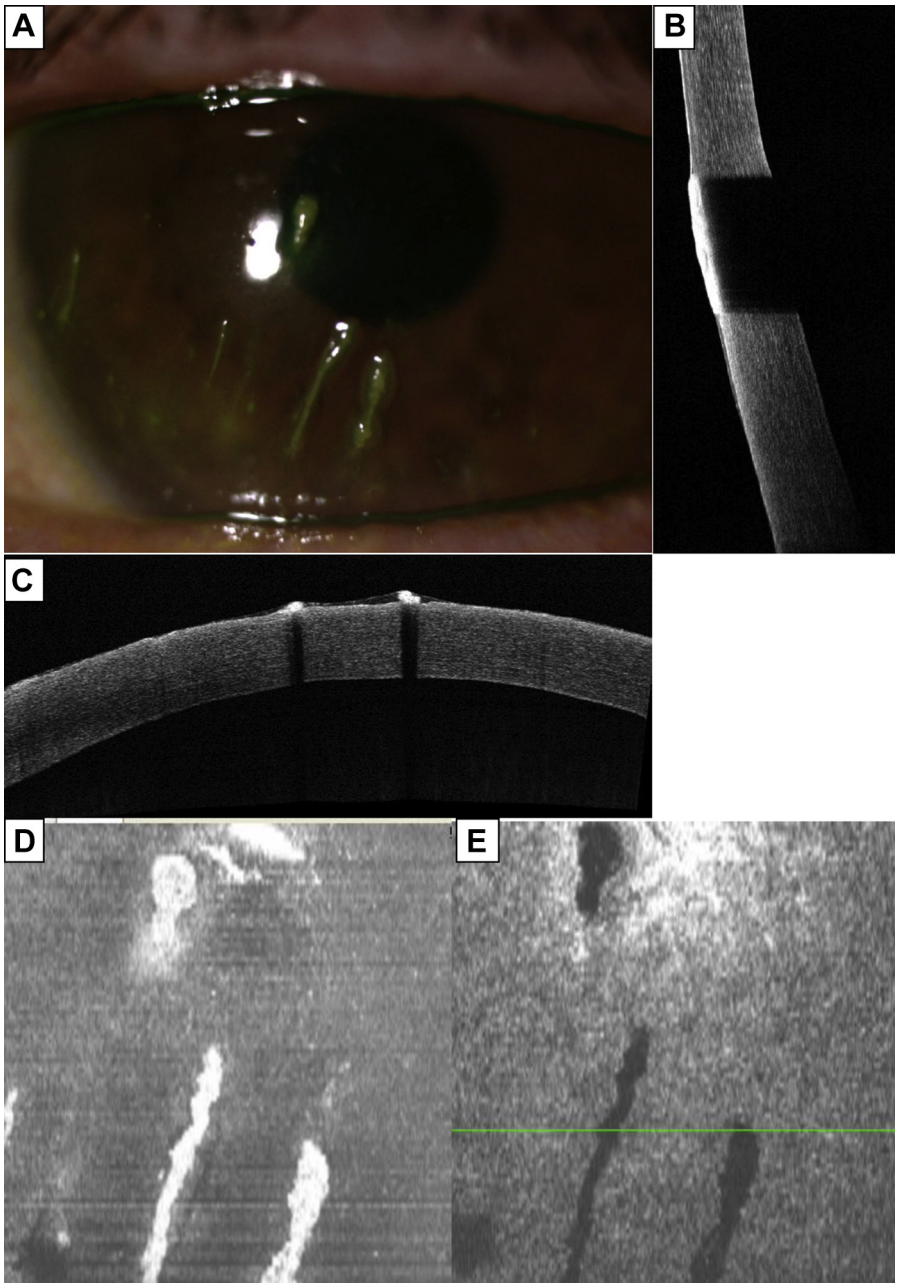

Figure 9. Filamentary keratitis. On slit-lamp examination, positively staining mucus filaments attached at one or both ends to the cornea can be noted (A). On AS-OCT, filaments appear as highly hyper-reflective deposits with a posterior shadowing (B and C). En-face images show the disposition of filaments (D and E).

D. Corneal Grafts

In a 42-year-old man with a central, post-traumatic corneal scar, B-scans were realized in different zones. Depending on the location of B-scans, the depth of the corneal scar was different (Figures 19A and 19B). C-scans allowed us to identify the exact location of the deepest point of the scar and consequently were useful to determine the depth of ablation during lamellar surgery (C).

B scans allowed analysis of the lateral graft-host junction and the interface after deep anterior lamellar keratoplasty (**DALK** [Figure 20 A and 20C]). On C-scans, a thick hyper-reflective line was observed as an evidence of a good graft host apposition at the graft-host junction (B), and consecutive C-scans allowed evaluation of the interface and the good apposition of the graft (D).

A case of Descemet's stripping endothelial keratoplasty (**DSEK**) is presented in Figure 21. B-scans were useful to evaluate the attachment of the endothelial graft to the host's posterior stroma. The regularity of the graft's edges and of the interface could be analyzed using en-face OCT.

As for DALK, en-face OCT allowed us to access the lateral junction of penetrating keratoplasty (Figure 22A) and also tissue changes such as Descemet's membrane folds (Figure 22B).

IV. DISCUSSION

Over the past two decades, knowledge of ocular surface diseases has greatly expanded through the use of AS-OCT and IVCM. Currently, these imaging modalities are widely

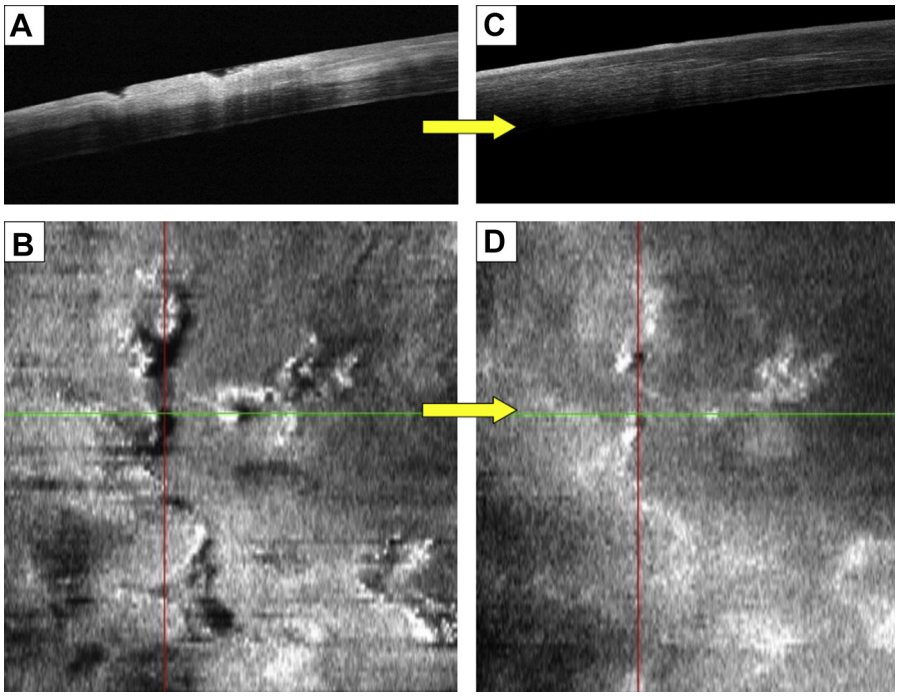

Figure 10. Herpetic keratitis. C-scans were taken initially and during follow-up at D1 (A and B) and D7 (C and D). During the follow-up, the ulcer resolved by approximation of its edges.

used in clinical practices to explore the ocular anterior-segment pathologies with their proper technical limits.[13,21-27] While the IVCM is a contact technique that provides data on a cellular level, the AS-OCT only provides cross-sectional anatomical images.[28] En-face OCT is a novel imaging modality derived from SD-OCT. It produces coronal sections, also called C-scans. These C-scans are oriented in a frontal plane, perpendicular to the optical axis of the eye. They give an instant overview of changes as a two-dimensional transversal slice at any given depth and may look confusing to an untrained observer, due to their high depth resolution and their frontal orientation through the ocular surface. Initially developed for retinal imaging, en-face OCT has provided a better understanding of the pathogenesis, diagnosis, and follow-up of several retinal diseases, such as age-related macular degeneration, central serous retinopathy, cystoid macular edema, epiretinal membrane, macular hole, and chronic solar retinopathy.[29-35]

To our knowledge, there are very few published papers reporting the use of en-face AS-OCT. In the first study, Lathrop et al used a prototype of en-face OCT to analyze the palisades of Vogt of 20 human donor corneal rims.[36] They showed that OCT was able to safely and effectively image palisades of Vogt. Recently, Hwang et al used another prototype system of en-face OCT to examine the meibomian glands in two healthy volunteers and seven patients with meibomian gland dysfunction.[37] A 3D reconstruction of meibomian glands was successfully achieved using high-speed en-face SD-OCT.

In our study, anterior segment en-face imaging was achieved with the RTVue®. Many other OCT devices are currently available. Table 2 summarizes and compares them in terms of technology, wavelength, resolution, scanning speed, scan depth, and availability of anterior segment en-face technology.

Herein, we describe several examples of the broad applications potentially provided by a commercially available, widely and routinely used OCT device. We compared en-face OCT images with those obtained with conventional B-scans and IVCM. Our observations using en-face OCT are well in agreement with previously reported B-scans, IVCM, and histopathologic findings. IVCM has been used to analyze many ocular surface diseases, like map-dot-fingerprint dystrophy,[38] but this technique requires direct contact with the eye, which may inadvertently cause more damage to an eye that is already fragile. OCT offers an alternative imaging modality, which eliminates this disadvantage. This new technique was capable of identifying corneal microstructural changes related to corneal dystrophies in patients, with no corneal contact. The C-scan images provided clear visualization of subepithelial multilaminar, linear, and curvilinear hyper-reflective lines. These findings were consistent with those of IVCM.[38] En-face OCT may thus be useful for noninvasive diagnosis and follow-up of map-dot-fingerprint corneal dystrophy and other similar basement membrane abnormalities.

En-face OCT can also be used to determine the size, depth, shape, and location of corneal opacities and deposits, as described in Reis-Bücklers corneal dystrophy, corneal cystinosis, and thesaurismosis. In comparison, B-scan OCTs do not allow visualization of these abnormalities so accurately. Although slit-lamp examination can provide a rough sense of deposit depth, en-face OCT provides

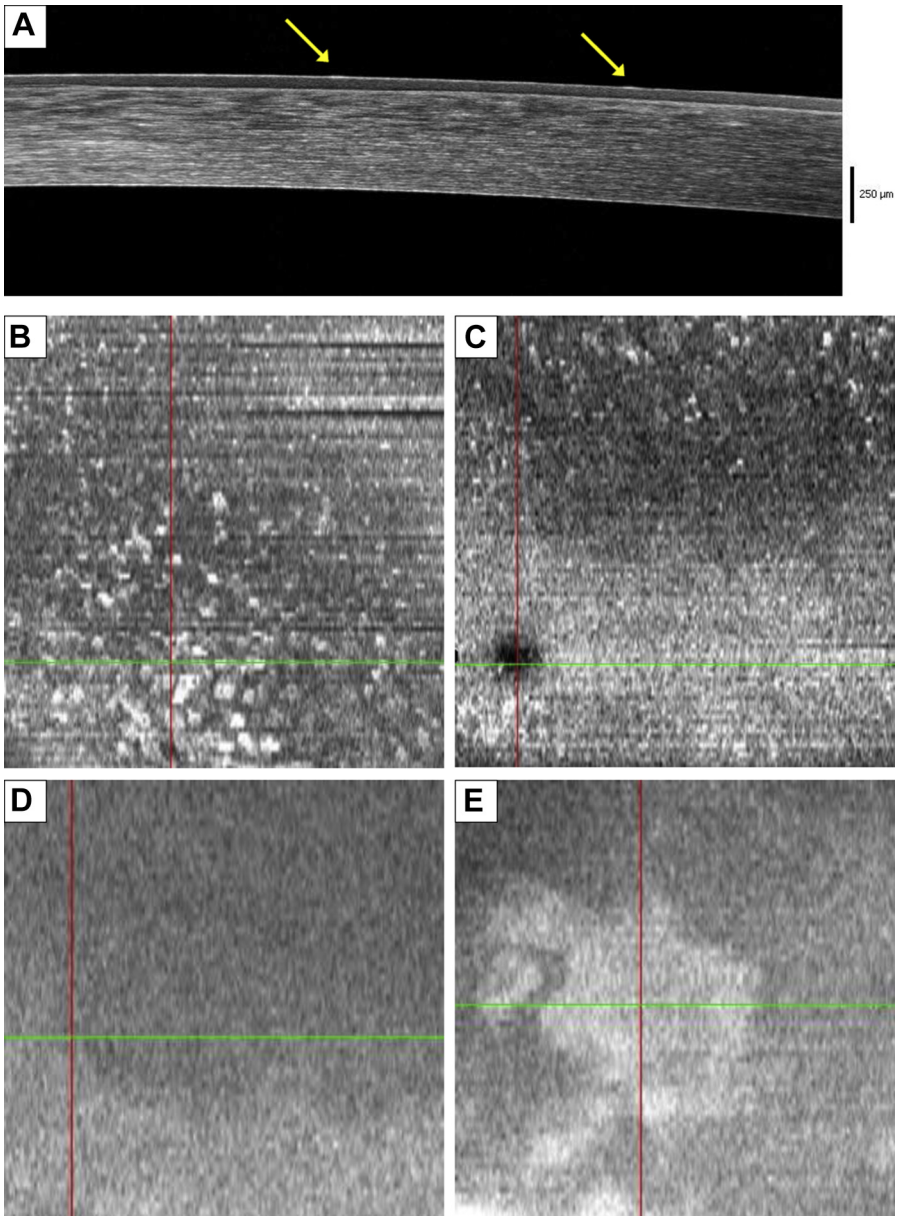

Figure 11. Rosacea. Orthogonal B-scans showed very discrete hyper-reflective structures in the tear film (A, yellow arrows). Superficial en-face scans showed superficial punctate lacrimal hyper-reflective structures in front of the superior cornea (B). These precorneal structures were larger and more numerous in front of the lower cornea (C). Deeper C-scans showed subepithelial hyper-reflective lesions corresponding to subepithelial infiltrates (E). En-face OCT did not show any precorneal hyper-reflective images in five normal control subjects (D).

high-resolution images in which the depth can be precisely measured. Furthermore, this imaging technique allows visualizing, locating, and precisely measuring the size of infectious keratitis without any direct contact with the cornea. Therefore, it could be useful to monitor the efficacy of treatments noninvasively.

We also used en-face OCT to explore various etiologies of keratitis. Herpetic epithelial dendritic keratitis showed an epithelial defect on C-scans. En-face OCT allowed the monitoring of the healing process in corneal herpetic ulcer. In contrast, dry eye keratitis corresponded to areas of intraepithelial hyper-reflectivity on C-scans. There was no epithelial defect despite the presence of fluorescein staining. We conclude that fluorescein staining does not necessarily correspond to an epithelial disruption and could correspond to areas of cellular damage or increased epithelial permeability to dyes.[39]

Meibomian gland dysfunction (**MGD**), also called posterior blepharitis, is a well-known cause of evaporative dry eye. In the present study, en-face OCT was used to evaluate the lacrimal film in rosacea, and we observed the presence of superficial lacrimal hyper-reflective structures that were larger and more frequent in front of the lower cornea. These hyper-reflective structures were not present in normal control subjects. According to previous reports,[40,41] these lacrimal structures are probably due to denser tears. In MGD, their concentration in front of the lower cornea is probably due to the effect of gravity. Moreover, MGD is associated with lid margin inflammation combined with the abnormal meibomian lipid delivery. Many authors reported that the tear-film lipid layer (**TFLL**) is particularly altered in MGD.[42-45] This layer is derived from meibomian lipids and is essential for the stability of normal tear film.

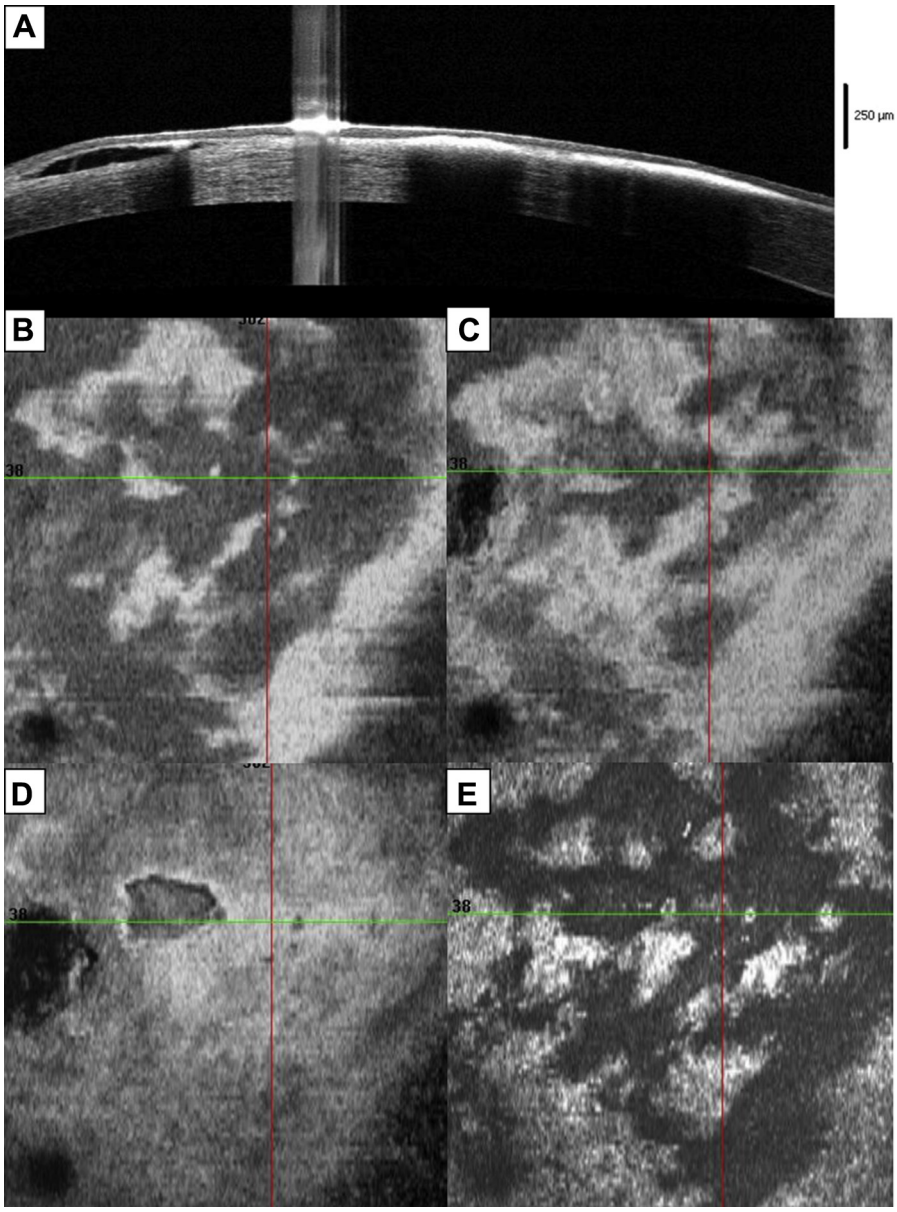

Figure 12. Band keratopathy. On the transversal B-OCT scan, highly hyperreflective intraepithelial deposits and hyporeflective cysts can be noted (A). En-face OCT showed the distribution of calcareous concretions (B to E).

Our findings are consistent with previous reports. Indeed, altered TFLL is associated with decreased tear film stability and concentration of dense tears in front of the lower cornea. These tears contain abundant pro-inflammatory cytokines and/or chemokines, which explains why further corneal damage and inflammatory infiltrations are more frequently found in the inferior cornea.

In our study, en-face anterior segment SD-OCT was also used to evaluate pterygium, which was correlated with the analysis by IVCM. On C-scans, we clearly identified the pterygium corneal limits, the pterygium stroma with its borders, and, in active pterygium, Fuchs patches. As previously reported, the presence of Fuchs patches is associated with pterygium activity, their visibility due to the presence of dendritic cells, which possibly participate in the activation of proliferation.[46,47] We hypothesize that the surface of these patches is correlated to the pterygium activity. B-scans allowed Fuchs patches to be visualized, but did not allow measurement of their surface. Thus, the use of en-face OCT could be useful to assess and quantify the activity of pterygium by evaluating the extent of these patches.

AS-OCT was also used to explore conjunctivochalasis. Vertical B-scans showed a conjunctival fold between the cornea and the lower eyelid in all cases. In most cases, consecutive OCT C-scans showed the presence of multiple, hyporeflective conjunctival cysts with septae. Interestingly, in one atypical case, we noted the presence of a deep conjunctival network. We hypothesize that this pattern could correspond to dilatation of the lymphatic network due to a downstream obstruction. Visualization of this pattern has been made possible by this new imaging technique. These cases show that the pathogenesis of

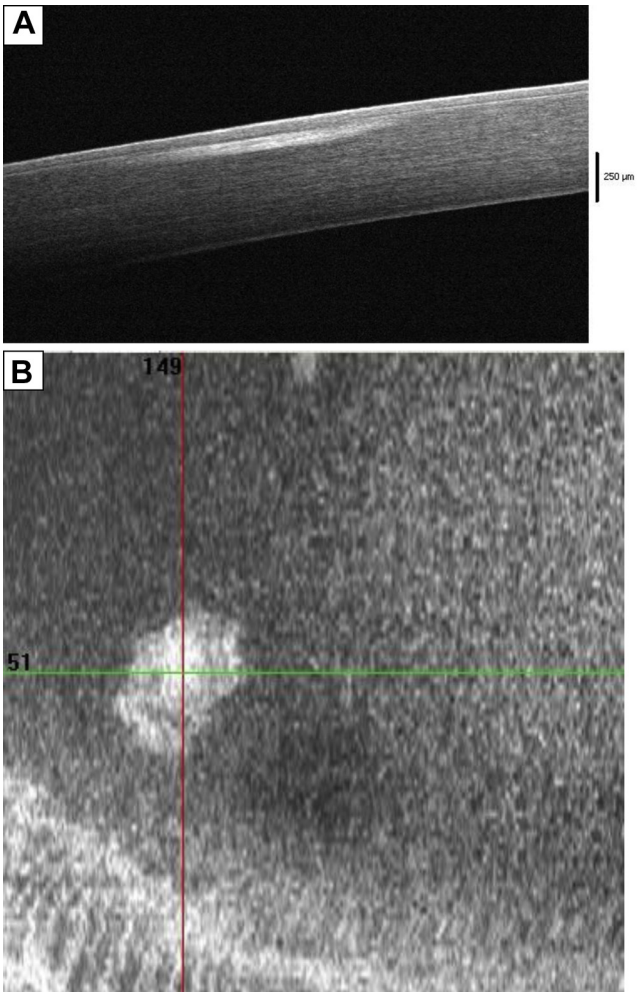

Figure 13. Peripheral sterile infiltrate. B-scan OCT showed peripheral corneal infiltrate (A). On C-scan, a superficial circular hyper-reflective area with clear visualization of limbal Vogt striae can be noted (B).

conjunctivochalasis is still unclear and needs further study for a more detailed understanding of this pathology.

Ocular surface squamous neoplasia (**OSSN**) is the most common conjunctival and limbal malignant tumor. Recently, IVCM and ultra-high-resolution AS-OCT were used for the diagnosis and management of OSSN.[48-51] En-face OCT supported B-scans and IVCM findings and gave us complementary information about the exact surface and the degree of the lateral extension of the tumor. The difference of reflectivity between OSSN and normal corneal epithelium facilitates the identification of the tumor's edges. We believe that en-face OCT could be useful for the follow-up of patients with OSSN or to detect relapses after treatment, particularly in case of conservative treatment by antimitotic eye drops.

Recently, AS-OCT was used to monitor lamellar surgeries, such as DALK and DSEK.[52-54] Through our examples, we demonstrate that en-face OCT provides supplementary information and could be useful for the preoperative and postoperative assessment of lamellar surgeries. Preoperatively, C-scans allowed us to determine the deepest point of corneal scar and its exact distance from the visual axis. Therefore, this imaging technique could give valuable information on the depth of corneal ablation in anterior lamellar keratoplasties. Postoperatively, en-face OCT could be useful for the follow-up of lamellar surgeries. As compared to B-scans, C-scans allow improved visualization of the graft host lateral junction, showing a thick hyper-reflective line as evidence of a good graft-host congruence. Consecutive C-scans also allow evaluation of the regularity of the interface and the absence of abnormal deposits in DALK and DSEK.

The major advantages of en-face OCT over IVCM include easy operation and rapid image acquisition. In addition, the non-contact method avoids patient discomfort and external pressure on the globe, which is especially useful in patients with corneal epithelium fragility, as in basement corneal dystrophy or in cases of infections or traumatic erosions. En-face OCT is undoubtedly safer than IVCM in the evaluation of corneal dystrophies because AS-OCT is a non-contact technique. Moreover, unlike IVCM, en-face OCT imaging can be centered over the pathologic area, using the concomitant video imaging.

Although the resolution of en-face OCT is lower than that of IVCM, it allows an overall analysis of the ocular surface due to larger visualization windows. In fact, the surface detected by en-face OCT (4×4 mm) is 100 times larger than

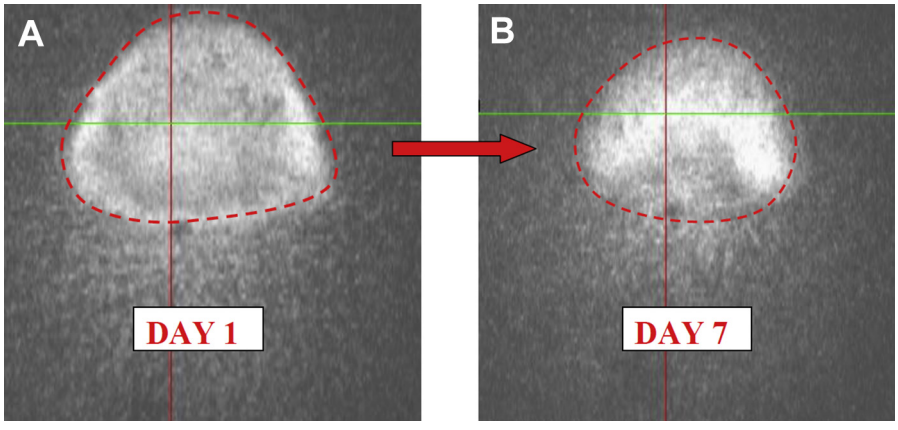

Figure 14. Infectious keratitis. On C-scans, infectious keratitis appears as an area of intrastromal hyper-reflectivity (A). Follow-up was possible by measuring the surface of infectious keratitis under treatment (B). The B scans showed the infiltration depth of the infectious keratitis (C and D).

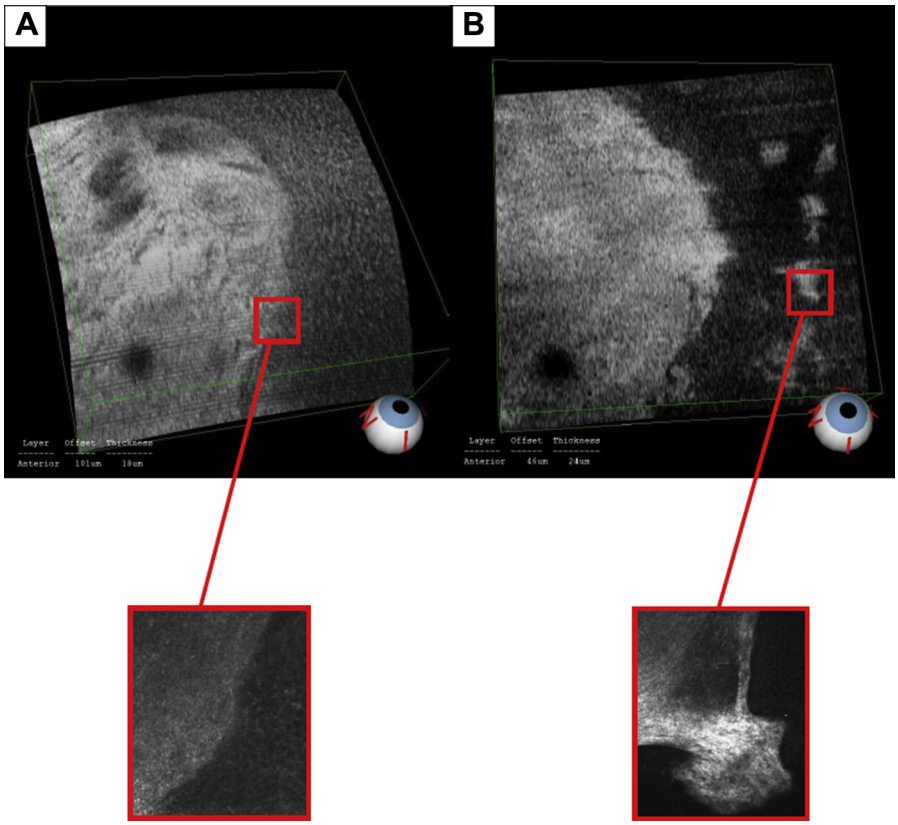

Figure 15. Pterygium. In this case of active pterygium, a hyper-reflective area in front of the tip of the pterygium (A) can be seen, which is correlated with the IVCM image (C). In inactive pterygium, there is no hyper-reflectivity in front of the tip the pterygium (B). IVCM of the margin of the pterygium (D).

the surface analyzed by IVCM (0.4×0.4 mm). IVCM is limited by high magnification that restricts the area of the scan. Therefore, it cannot provide overall visualization of the ocular surface. En-face OCT makes these "macroscopic views" possible for the first time.

Compared to conventional transversal scans, en face OCT allows a complementary and a different angle imaging of ocular surface structures. Visualization in a frontal plane can reveal some details that are sometimes not easily discernible in B-scans. Combining these various imaging

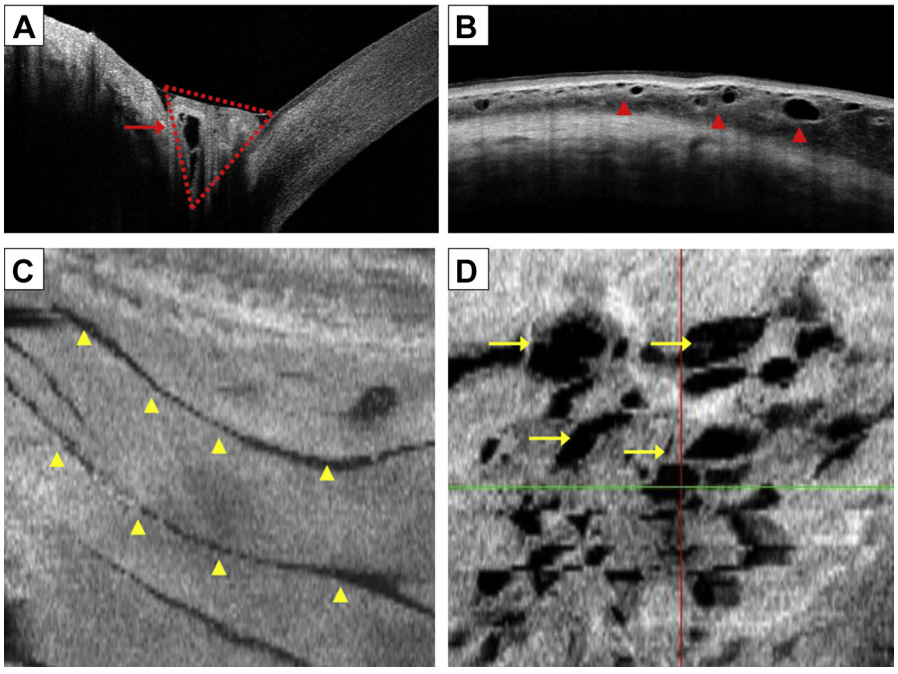

Figure 16. Typical conjunctivochalasis. Vertical B-scan shows a triangular conjunctival fold between the cornea and the lower eyelid (A, red arrow). On transversal B-scan, conjunctival cysts can be noted (B, red arrowheads). Consecutive OCT C-scans show superficial linear folds (C, yellow arrowheads) and deeper, multiple, hyporeflective conjunctival cysts with septae (D, yellow arrows).

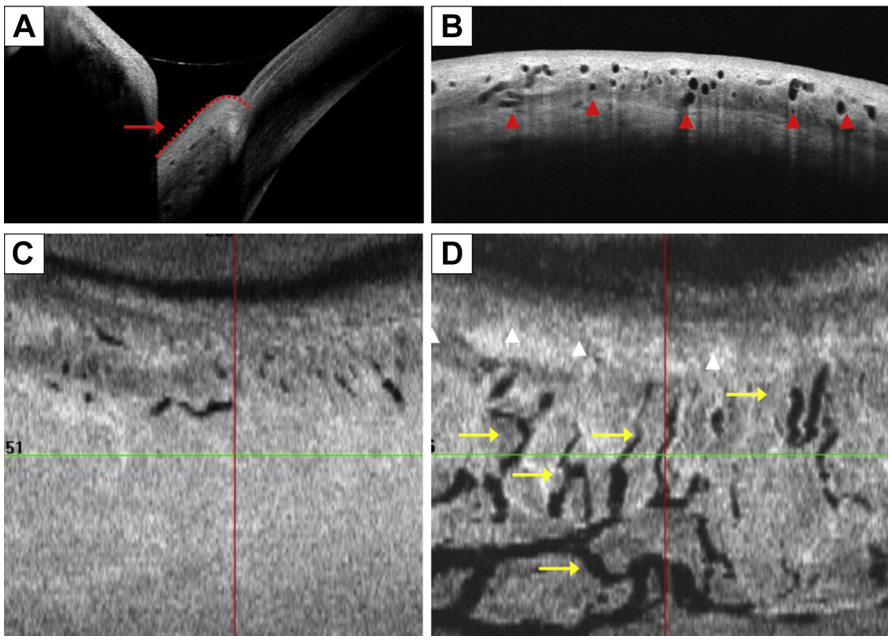

Figure 17. Atypical conjunctivochalasis. The vertical B-scan shows a semicircular conjunctival fold between the cornea and the lower eyelid (A, red arrow). On the transversal B-scan, conjunctival cysts can be seen (B, red arrowheads). On the C-scan, the cysts seen on conventional scans are actually sections of an organized network (C and D, yellow arrows).

techniques could provide complementary information and reveal supplemental morphological details in patients with ocular surface conditions.[38] This may improve the quality of diagnosis and follow-up and help to better understand anterior segment pathological processes. Table 3 summarizes and compares these three complementary imaging modalities.

The RTVue® en-face AS-OCT nonetheless has some limitations. First, the currently available software automatically identifies the boundaries, and they cannot be drawn manually. Sometimes the cornea may be shadowed by eyelashes or the OCT signal may be low in the peripheral cornea. Under these circumstances, the RTVue® software may misidentify the corneal boundaries and induce a mismatch of curvature

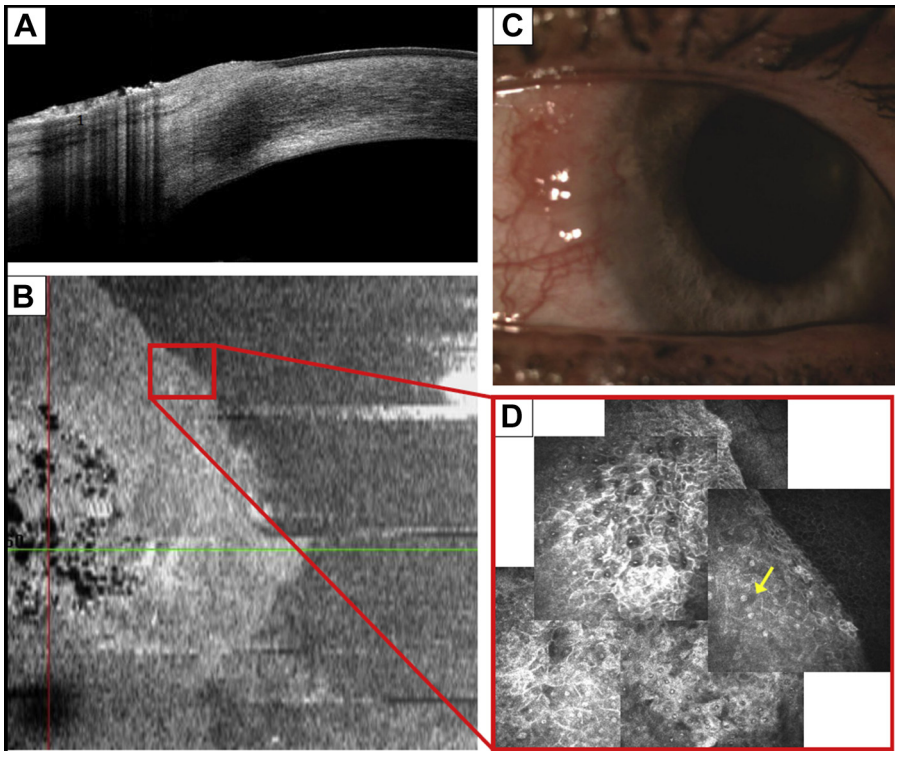

Figure 18. Ocular surface squamous neoplasia. B-scan shows a hyper-reflective thickened epithelium and an abrupt transition between a normal and abnormal corneal epithelium (A). On C-scan, the lesion is hyper-reflective with clearly visible edges and centered by highly hyper-reflective superficial deposits corresponding to keratinization (B). On slit-lamp examination, there is a limbic, nonspecific lesion (C). A reconstruction of IVCM images shows abnormal hyper-reflective tumoral cells (yellow arrow, D).

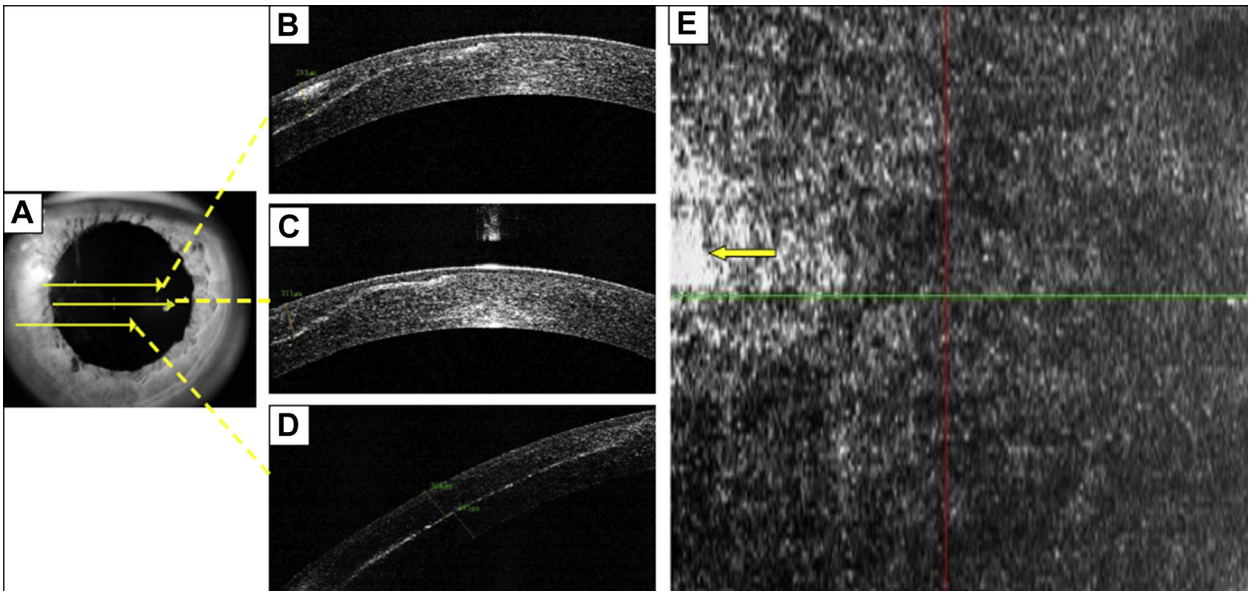

Figure 19. Pre-operative assessment of a corneal scar. The deepest point of the scar varies with the location of B-scans (A-D). C-scans allowed us to identify the exact location of the deepest point of this corneal lesion (yellow arrow) (E).

between the scanning arc and the curvature of the ocular surface. Future improvements in software will allow manual drawing of the boundaries, thus overcoming this problem.

Unlike IVCM, which has established validity in diagnosing specific pathogens,[55-57] en-face OCT still has a lower resolution that makes identification of specific

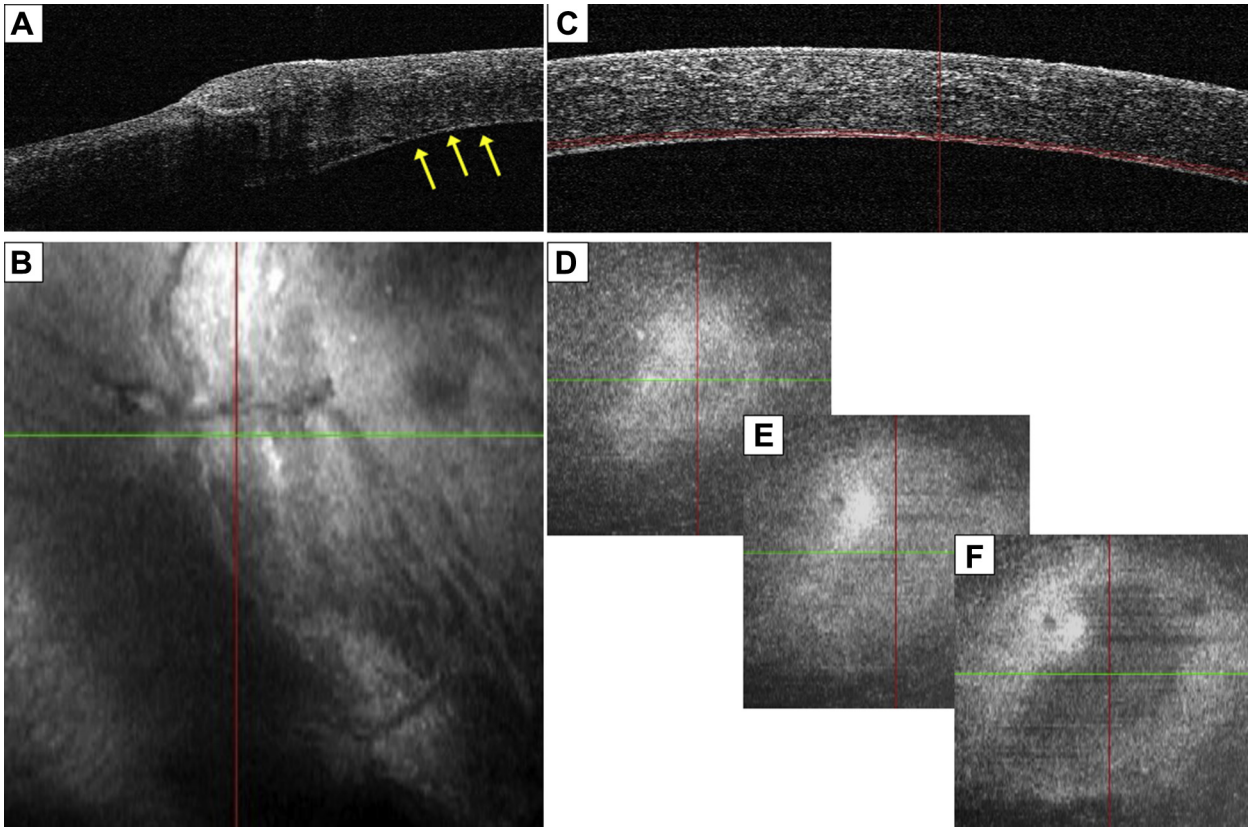

Figure 20. Deep anterior lamellar keratoplasty. B-scan centered on the lateral graft-host junction shows good apposition with no interface fluid and could identify a normal thin interface (yellow arrows). Corresponding C-scan shows a thick hyper-reflective line as evidence of good graft-host apposition at the lateral graft-host junction (B). Figure C shows a B-scan acquired in the center of the graft. The red boundaries represent the plane of the C-scan and are centered on the host-graft interface. Corresponding consecutive C-scans allow analysis of the interface and the good apposition of the graft (D).

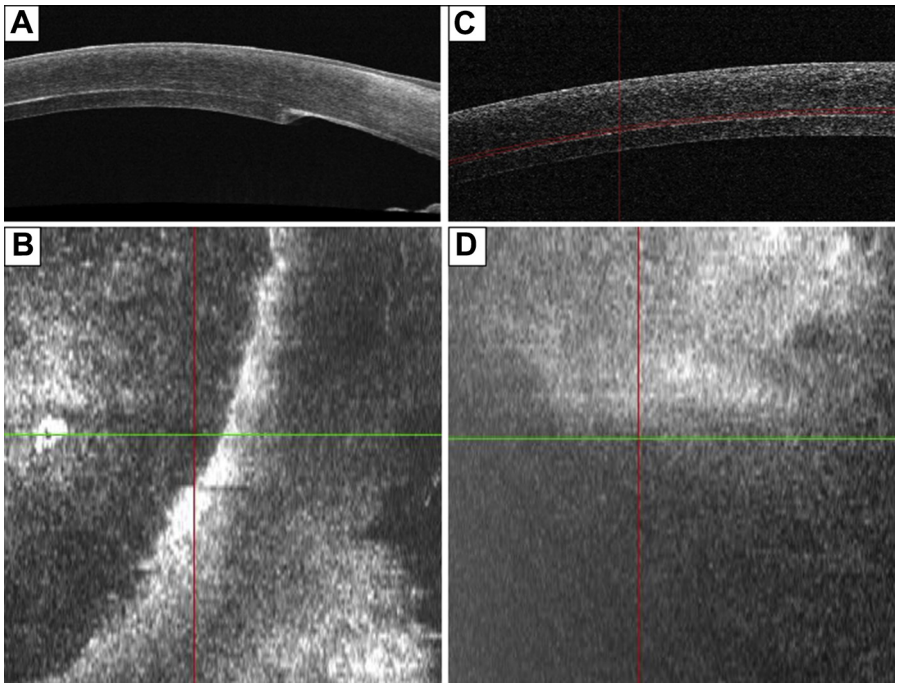

Figure 21. Descemet's stripping endothelial keratoplasty. B-scans show the good attachment of the endothelial graft to the host's posterior stroma (A and C). En-face OCT allows analysis of the graft's border (B) and assessment of the regularity of the interface (D).

pathogens impossible. Furthermore, the inability of en-face OCT to image deeper lesions and to "see through" an overlying opacification could restrict its usefulness as compared to IVCM.

Another limitation of RTVue® is the lack of availability of an eye-tracking system. Therefore, any ocular micromovement may induce a motion artifact. The use of an external fixation target could reduce these artifacts. We recommend recapturing the OCT volume if the quality of the OCT images is poor and/or the corneal surface boundaries are misidentified.

Finally, the current software attached to OCT could not measure the distances and surfaces exactly, and we had to combine this software with external software to access the surface of corneal abscesses.

Overall, none of these limitations prevented us from obtaining high-quality images, and in our experience, en-face OCT is a promising imaging technique. Future improvement in software could be envisaged to make the acquisition and processing of images simpler.

V. CONCLUSION

This study shows that en-face OCT is a promising adjunctive tool for assessing a wide variety of ocular surface conditions. It can noninvasively provide additional information not readily available with conventional imaging techniques. This capability has the potential to provide greater insight into the understanding and follow-up of ocular surface conditions. With continued improvements to the

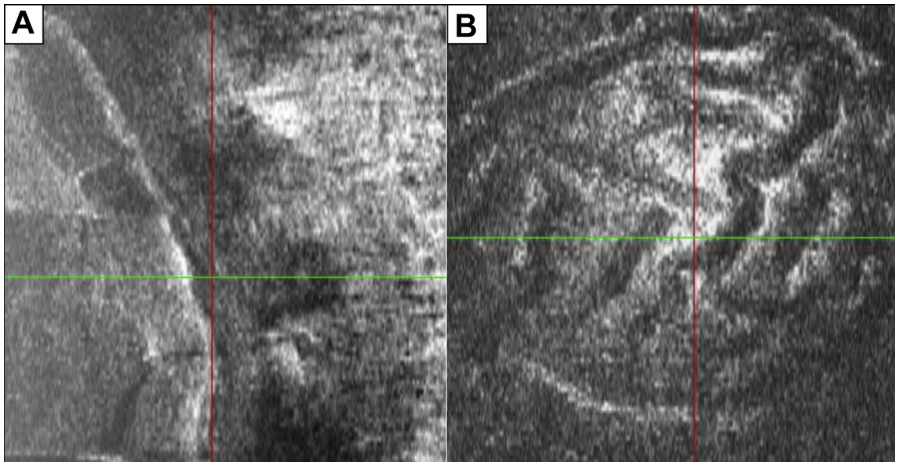

Figure 22. Penetrating keratoplasty. On C-scan, the graft-host lateral junction is clearly identified; the absence of defect and the presence of a hyper-reflective line demonstrate the good congruence of this junction (A). En-face OCT also allowed the visualization of Descemet's membrane folds (B).

Table 2. Comparison of currenty available anterior segment OCT devices (listed alphabetically by manufacturer).

Device	Manufacturer	Technology	Wavelength (nm)	Axial resolution (μm)	Transverse resolution (μm)	Scanning speed (A scans/sec)	Scan depth (mm)	Commercially available	Anterior segment en-face technology
Bioptigen Envisu SDOIS C-2200	Bioptigen Inc.	SD	HR source 840 nm VHR source 870 nm	HR source: <6 VHR source: <4	9 to 25	32000	1.7	Yes	No
Bioptigen Envisu SDOIS C-2300	Bioptigen Inc.	SD	HR source 840 nm VHR source 870 nm	HR source: <6 VHR source: <4	9 to 25	32000	2.5	Yes	No
OCT HS-100	Canon	SD	855	3	20	70000	2	Yes	No
Visante OCT	Carl Zeiss Meditec	TD	1310	18	60	2000	6	Yes	No
Stratus OCT	Carl Zeiss Meditec	TD	840	10	20-25	400	2	Yes	No
Cirrus HD-OCT	Carl Zeiss Meditec	SD	840	5	15	27000	2	Yes	Yes
SL-OCT	Heidelberg Engineering	TD	1310	25	100	200	7	Yes	No
Spectralis OCT	Heidelberg Engineering	SD	820	7	14	40000	1.9	Yes	No
SOCT Copernicus	Optopol	SD	840	6	12 to 18	25000	2	Yes	No
SOCT Copernicus +	Optopol	SD	830	5	12 to 18	27000	2	Yes	No
SOCT Copernicus HR	Optopol	SD	850	3	12 to 18	52000	NS	Yes	No
OCT SLO	Optos	SD	830	<6	20	27000	2	Yes	No
RTVue	Optovue	SD	830	5	15	26000	3	Yes	Yes
iVue	Optovue	SD	840	5	15	26000	2 to 2.3	Yes	Yes
Avanti Rtvue XR	Optovue	SD	840	5	NS	70000	3	Yes	Yes
3D OCT-2000	Topcon	SD	840	5 to 6	20	27000 in US 50,000 outside US	2.3	Yes	Yes
3D OCT-1 Maestro	Topcon	SD	NS	6	20	50000	NS	Yes	Yes
Ultra high-resolution OCT	Custom-built device	SD	500 to 1600	2 to 3	Approximately 6	24000 to 26000	1.5 to 4	No	Yes

HR: High resolution; NS: Not specified; SD: Spectral domain; TD: Time domain; US: United States; VHR: Very high resolution.

Table 3. Comparison of en-face anterior-segment OCT, B-scans, and in vivo confocal microscopy.

	En-face anterior-segment OCT	Conventional B-scans OCT	In vivo confocal microscopy
Analyzed plane	Frontal	Transversal	Frontal
Examination mode	Non-contact	Non-contact	Contact
Surface area analyzed	Adjustable from 1×1 mm to 8×8 mm	Adjustable from 1 to 8 mm	400×400 µm
Difficulty of image acquisition	Minimal experience is required for image acquisition	Minimal experience is required for image acquisition	Image acquisition is more difficult and operator-dependent
Resolution	Axial resolution, 5 µm Transversal resolution, 15 µm	Axial resolution, 5 µm Transversal resolution, 15 µm	Axial resolution, 2 µm Transversal resolution, 4 µm
Other characteristics	Inability to image deeper lesions in the presence of overlying opacification	Inability to image deeper lesions in the presence of overlying opacification	Established validity in diagnosing some specific pathogens[55-57]

technology, future development of en-face ultra-high-resolution (**UHR**) OCT will improve resolution and enhance the sensitivity and specificity of this new technology, allowing earlier diagnosis and more reliable follow-up.

REFERENCES

1. Huang D, Swanson EA, Lin CP, et al. Optical coherence tomography. *Science* 1991;254:1178-81
2. Izatt JA, Hee MR, Swanson EA, et al. Micrometer-scale resolution imaging of the anterior eye in vivo with optical coherence tomography. *Arch Ophthalmol* 1994;112:1584-9
3. Lee KS, Sung KR, Shon K, et al. Longitudinal changes in anterior segment parameters after laser peripheral iridotomy assessed by anterior segment optical coherence tomography. *Invest Ophthalmol Vis Sci* 2013;54:3166-70
4. Konstantopoulos A, Yadegarfar ME, Yadegarfar G, et al. Deep sclerectomy versus trabeculectomy: a morphological study with anterior segment optical coherence tomography. *Br J Ophthalmol* 2013;97:708-14
5. Fukuda R, Usui T, Miyai T, et al. Tear meniscus evaluation by anterior segment swept-source optical coherence tomography. *Am J Ophthalmol* 2013;155:620-4
6. Ramos JL, Li Y, Huang D. Clinical and research applications of anterior segment optical coherence tomography — a review. *Clin Experiment Ophthalmol* 2009;37:81-9
7. Rocha KM, Perez-Straziota CE, Stulting RD, et al. SD-OCT analysis of regional epithelial thickness profiles in keratoconus, postoperative corneal ectasia, and normal eyes. *J Refract Surg* 2013;29:173-9
8. Perera SA, Ho CL, Aung T, et al. Imaging of the iridocorneal angle with the RTVue spectral domain optical coherence tomography. *Invest Ophthalmol Vis Sci* 2012;53:1710-3
9. Pang CE, Vanathi M, Tan DT, Mehta JS. Evaluation of corneal epithelial healing under contact lens with spectral-domain anterior segment optical coherence tomography (SD-OCT). *Open Ophthalmol J* 2011;5:51-4
10. Singh M, See JL, Aquino MC, et al. High-definition imaging of trabeculectomy blebs using spectral domain optical coherence tomography adapted for the anterior segment. *Clin Experiment Ophthalmol* 2009;37:345-51
11. Kealey P, Talarico J. Optovue announces FDA aproval for corneal power measurements. http://www.optovue.com/wp-content/uploads/Press-Release-Corneal-Power.pdf (2011)
12. Siqueira RC, Nogueira MC. Identifying early recurrence of choroidal neovascularization during treatment with ranibizumab using C-scan. *Eur J Ophthalmol* 2010;20:559-64
13. Drexler W, Fujimoto JG. State-of-the-art retinal optical coherence tomography. *Prog Retin Eye Res* 2008;27:45-88
14. Optovue, Inc. RTVue Overview. Optovue Web site: http://www.optovue.com/products/rtvue. Accessed 04 August 2013
15. Cogan DG, Donaldson DD, Kuwabara T, et al. Microcystic dystrophy of the corneal epithelium. *Trans Am Ophthalmol Soc* 1964;62:213-25
16. Cogan DG, Kuwabara T, Donaldson DD, et al. Microcystic dystrophy of the cornea: a partial explanation for its pathogenesis. *Arch Ophthalmol* 1974;92:470-4
17. Kuchle M, Green WR, Volcker HE, et al. Reevaluation of corneal dystrophies of Bowman's layer and the anterior stroma (Reis-Bucklers and Thiel-Behnke types): a light and electron microscopic study of eight corneas and a review of the literature. *Cornea* 1995;14:333-54
18. Severin M, Kirchhof B. Recurrent Salzmann's corneal degeneration. *Graefes Arch Clin Exp Ophthalmol* 1990;228:101-4
19. Meyer JC, Quantock AJ, Thonar EJ, et al. Characterization of a central corneal cloudiness sharing features of posterior crocodile shagreen and central cloud dystrophy of François. *Cornea* 1996;15:347-54
20. Belliveau MJ, Brownstein S, Agapitos P, et al. Ultrastructural features of posterior crocodile shagreen of the cornea. *Surv Ophthalmol* 2009;54:569-75
21. Masters BR, Bohnke M. Confocal microscopy of the human cornea in vivo. *Int Ophthalmol* 2001;23:199-206
22. Jalbert I, Stapleton F, Papas E, et al. In vivo confocal microscopy of the human cornea. *Br J Ophthalmol* 2003;87:225-36
23. Zhivov A, Stachs O, Kraak R, et al. In vivo confocal microscopy of the ocular surface. *Ocul Surf* 2006;4:81-93
24. Labbé A, Khammari C, Dupas B, et al. Contribution of in vivo confocal microscopy to the diagnosis and management of infectious keratitis. *Ocul Surf* 2009;7:41-52
25. Mantopoulos D, Cruzat A, Hamrah P. In vivo imaging of corneal inflammation: new tools for clinical practice and research. *Semin Ophthalmol* 2010;25:178-85
26. Simpson T, Fonn D. Optical coherence tomography of the anterior segment. *Ocul Surf* 2008;6:117-27
27. Jancevski M, Foster CS. Anterior segment optical coherence tomography. *Semin Ophthalmol* 2010;25:317-23

28. Alhatem A, Cavalcanti B, Hamrah P. In vivo confocal microscopy in dry eye disease and related conditions. *Semin Ophthalmol* 2012;27:138-48
29. van Velthoven ME, de Vos K, Verbraak FD, et al. Overlay of conventional angiographic and en-face OCT images enhances their interpretation. *BMC Ophthalmology* 2005;5:12
30. van Velthoven ME, Verbraak FD, Garcia PM, et al. Evaluation of central serous retinopathy with en face optical coherence tomography. *Br J Ophthalmol* 2005;89:1483-8
31. Chen RW, Gorczynska I, Srinivasan VJ, et al. High-speed ultrahigh-resolution optical coherence tomography findings in chronic solar retinopathy. *Retin Cases Brief Rep* 2008;2:103-5
32. Srinivasan VJ, Adler DC, Chen Y, et al. Ultrahigh-speed optical coherence tomography for three-dimensional and en face imaging of the retina and optic nerve head. *Invest Ophthalmol Vis Sci* 2008;49:5103-10
33. Wanek J, Zelkha R, Lim JI, et al. Feasibility of a method for en face imaging of photoreceptor cell integrity. *Am J Ophthalmol* 2011;152:807-14
34. Wolff B, Matet A, Vasseur V, et al. En face OCT imaging for the diagnosis of outer retinal tubulations in age-related macular degeneration. *J Ophthalmol* 2012;2012:542417
35. Sohrab M, Wu K, Fawzi AA. A pilot study of morphometric analysis of choroidal vasculature in vivo, using en face optical coherence tomography. *PLoS One* 2012;7:e48631
36. Lathrop KL, Gupta D, Kagemann L, et al. Optical coherence tomography as a rapid, accurate, noncontact method of visualizing the palisades of Vogt. *Invest Ophthalmol Vis Sci* 2012;53:1381-7
37. Hwang HS, Shin JG, Lee BH, et al. In vivo 3D meibography of the human eyelid using real time imaging Fourier-Domain OCT. *PLoS One* 2013;8:e67143
38. Labbé A, Nicola RD, Dupas B, et al. Epithelial basement membrane dystrophy: evaluation with the HRT II Rostock Cornea Module. *Ophthalmology* 2006;113:1301-8
39. Alarcon I, Tam C, Mun JJ, et al. Factors impacting corneal epithelial barrier function against Pseudomonas aeruginosa traversal. *Invest Ophthalmol Vis Sci* 2011;52:1368-77
40. Lee H, Min K, Kim EK, et al. Minocycline controls clinical outcomes and inflammatory cytokines in moderate and severe meibomian gland dysfunction. *Am J Ophthalmol* 2012;154:949-57
41. Bron AJ, Yokoi N, Gaffney EA, et al. A solute gradient in the tear meniscus. II. Implications for lid margin disease, including meibomian gland dysfunction. *Ocul Surf* 2011;9:92-7
42. Foulks GN, Bron AJ. Meibomian gland dysfunction: a clinical scheme for description, diagnosis, classification, and grading. *Ocul Surf* 2003;1:107-26
43. Joffre C, Souchier M, Grégoire S, et al. Differences in meibomian fatty acid composition in patients with meibomian gland dysfunction and aqueous-deficient dry eye. *Br J Ophthalmol* 2008;92:116-9
44. Finis D, Pischel N, Schrader S, Geerling G. Evaluation of lipid layer thickness measurement of the tear film as a diagnostic tool for Meibomian gland dysfunction. *Cornea* 2013;32:1549-53
45. Eom Y, Lee JS, Kang SY, et al. Correlation between quantitative measurements of tear film lipid layer thickness and meibomian gland loss in patients with obstructive meibomian gland dysfunction and normal controls. *Am J Ophthalmol* 2013;155:1104e2-10e2
46. Gheck L, Dupas B, Denion E, et al. Advantages of the in vivo confocal microscope for investigation of the pterygium. *J Fr Ophtalmol* 2007;30:703-10
47. Labbé A, Gheck L, Iordanidou V, et al. An in vivo confocal microscopy and impression cytology evaluation of pterygium activity. *Cornea* 2010;29:392-9
48. Thomas BJ, Galor A, Nanji AA, et al. Ultra high-resolution anterior segment optical coherence tomography in the diagnosis and management of ocular surface squamous neoplasia. *Ocul Surf* 2014;12:46-58
49. Kieval JZ, Karp CL, Abou Shousha M, et al. Ultra-high resolution optical coherence tomography for differentiation of ocular surface squamous neoplasia and pterygia. *Ophthalmology* 2012;119:481-6
50. Shousha MA, Karp CL, Canto AP, et al. Diagnosis of ocular surface lesions using ultra-high-resolution optical coherence tomography. *Ophthalmology* 2013;120:883-91
51. Tahiri Joutei Hassani R, Brasnu E, Amar N, et al. Contribution of in vivo confocal microscopy to diagnosis of invasive ocular surface squamous neoplasia: A case report. *J Fr Ophtalmol* 2010;33:163-8
52. Lim LS, Aung HT, Aung T, Tan DT. Corneal imaging with anterior segment optical coherence tomography for lamellar keratoplasty procedures. *Am J Ophthalmol* 2008;145:81-90
53. Hurmeric V, Wang J, Kymionis GD, Yoo SH. Persistent lamellar interface fluid with clear cornea after Descemet stripping automated endothelial keratoplasty. *Cornea* 2011;30:1485-7
54. Combillet F, Touboul D, Leger F, Colin J. Granular corneal dystrophy treated with deep anterior lamellar keratoplasty: comparing histological analysis and optical coherence tomography. *J Fr Ophtalmol* 2012;35:50.e1-5
55. Kobayashi A, Ishibashi Y, Oikawa Y. In vivo and ex vivo laser confocal microscopy findings in patients with early-stage acanthamoeba keratitis. *Cornea* 2008;27:439-45
56. Zhang X, Sun X, Jiang C, et al. A new in vivo confocal microscopy prognostic factor in Acanthamoeba keratitis. *J Fr Ophtalmol* 2014;37:130-7
57. Takezawa Y, Shiraishi A, Noda E, et al. Effectiveness of in vivo confocal microscopy in detecting filamentous fungi during clinical course of fungal keratitis. *Cornea* 2010;29:1346-52